N-Terminomic Changes of Neurons During Excitotoxicity Reveals Proteolytic Events Associated with Synaptic Dysfunctions and Potential Targets for Neuroprotection

Graphical Abstract

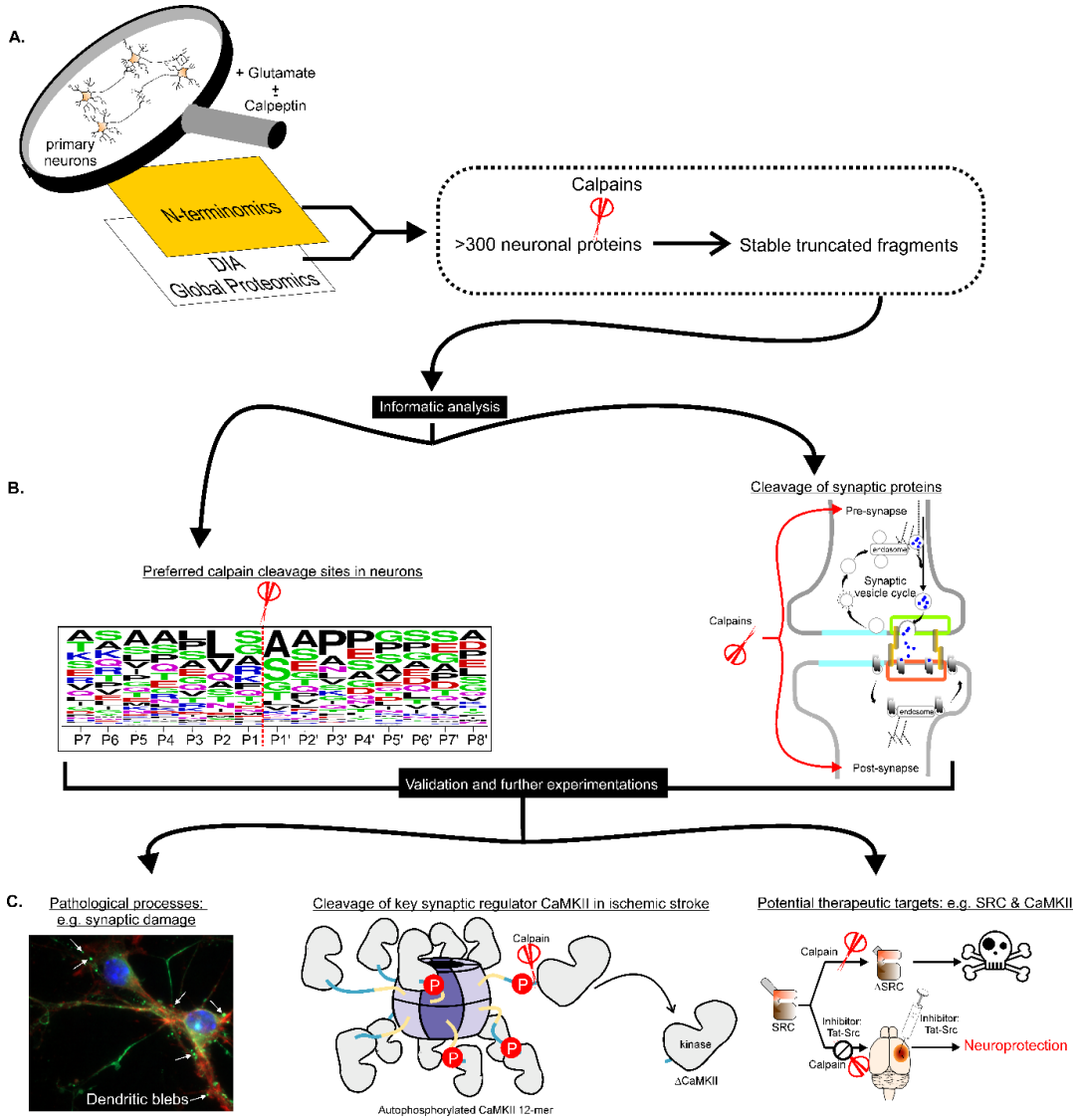

Authors
Sadia Ameen, Nane Griem-Krey, Antoine Dufour, … Giuseppe D. Ciccotosto, Nicholas A. Williamson, Cheng-Seng Ang and Heung-Chin Cheng

In Brief

Ameen, et al. used an N-terminomic method to identify neuronal proteins and the exact cleavage sites proteolyzed by calpains during excitotoxicity. Upon proteolysis, these proteins generate stable truncated fragments, which potentially induce synaptic dysfunction and loss, eventually leading to neuronal death. As such, some of these proteins such as protein kinases Src and CaMKII are potential targets for neuroprotection.

Highlights

- Over 300 neuronal proteins are cleaved by calpains to form stable truncated fragments during excitotoxicity.
- The calpain cleavage sites of these proteins unveil for the first time the preferred cleavage sequences of calpains in neurons.
- These pathological proteolytic events potentially induce synaptic dysfunction and loss, which leads to excitotoxic neuronal death.
- Some of the neuronal proteins proteolyzed by calpains are potential targets of neuroprotection.

Title:

N-Terminomic Changes of Neurons During Excitotoxicity Reveals Proteolytic Events Associated with Synaptic Dysfunctions and Potential Targets for Neuroprotection

Authors:

S. Sadia Ameen,[1,2] Nane Griem-Krey[3], Antoine Dufour,[4] M. Iqbal Hossain,[1,2] Ashfaqul Hoque,[5] Sharelle Sturgeon,[6] Harshal Nandurkar,[6] Dominik F. Draxler,[6] Robert L. Medcalf,[6] Mohd Aizuddin Kamaruddin,[1,2] Isabelle S. Lucet, [7,8] Michael G. Leeming,[2] Dazhi Liu,[9] Amardeep Dhillon,[10] Jet Phey Lim,[10] Faiza Basheer[10], Hong-Jian Zhu,[11] Laita Bokhari,[1,2] Carli Roulston,[12] Prasad N. Paradkar,[13] Oded Kleifeld,[14] Andrew N. Clarkson[15], Petrine Wellendorph[3], Giuseppe, D. Ciccotosto,[1,2]* Nicholas A. Williamson,[2]* Ching-Seng Ang[2]* and Heung-Chin Cheng[1,2]*

Affiliations:

[1]Department of Biochemistry and Pharmacology,[2]Bio21 Molecular Science and Biotechnology Institute, University of Melbourne, Parkville, Victoria 3052, Australia, [3]Department of Drug Design and Pharmacology, Faculty of Health and Medical Sciences, University of Copenhagen, DK-2100 Copenhagen, Denmark, [4]Department of Physiology and Pharmacology, University of Calgary, Calgary, Canada, T2N 4N1, Canada, [5]St. Vincent's Institute for Medical Research, Fitzroy, Victoria 3065, Australia, [6]Australian Centre for Blood Diseases, Monash University, Prahran, Victoria 3004, Australia, [7]Chemical Biology Division, The Walter and Eliza Hall Institute for Medical Research, Parkville, Victoria 3052, Australia, [8]Department of Medical Biology, University of Melbourne, Parkville, Victoria, 3052, Australia, [9]Department of Neurology, School of Medicine, University of California, Davis, CA 95616, USA, [10]School of Medicine, Faculty of Health, Deakin University, Waurn Ponds, Victoria 3216, Australia, [11]Department of Surgery (Royal Melbourne Hospital), University of Melbourne, Parkville, Victoria 3052, Australia, [12]Florey Institute of Neuroscience and Mental Health, Parkville, Victoria 3052, Australia, [13]CSIRO Health & Security, Australian Centre for Disease Preparedness, 5 Portarlington Road, East Geelong Vic 3220, Australia, [14]Faculty of Biology, Technion-Israel Institute of Technology, Biology Building, Technion City, Haifa 3200003, Israel, [15]Department of Anatomy, Brain Health Research Centre and Brain Research New Zealand, University of Otago, 9054 Dunedin, New Zealand

*Send all correspondence to:
Giuseppe Ciccotosto, email: j.ciccotosto@unimelb.edu.au
Nicholas Williamson, e-mail: nawill@unimelb.edu.au
Ching-Seng Ang, e-mail: ching-seng.ang@unimelb.edu.au
Heung-Chin Cheng, e-mail: heung@unimelb.edu.au

Abstract:

Excitotoxicity is a neuronal death process initiated by over-stimulation of ionotropic glutamate receptors. Although dysregulation of proteolysis and protein phosphorylation signaling networks is critical for excitotoxicity, the identity of affected proteins and mechanisms by which they induce neuronal cell death remains unclear. To address this, we used quantitative N-terminomics to identify proteins modified by proteolysis in neurons undergoing excitotoxic cell death. Our investigation led to the discovery of proteins that, upon proteolysis by calpains, perturb synaptic organization and function. These included key synaptic regulatory proteins including CRMP2, doublecortin-like kinase I, Src tyrosine kinase and calmodulin-dependent protein kinase IIβ (CaMKIIβ), which we found to undergo calpain-catalyzed proteolytic processing to generate stable truncated fragments with altered activities. We further show that blockade of proteolysis of Src by calpains could protect against neuronal loss in a rat model of neurotoxicity, and that CaMKIIβ and its isoform CaMKIIα undergo differential processing by calpains in mouse brains under physiological conditions and during ischemic stroke. Our findings thus reveal new insights into excitotoxic neuronal death mechanisms and suggest potential therapeutic targets for neurological disorders.

(177 words)

One Sentence Summary: Proteolytic events important for excitotoxic neuronal death as potential novel therapeutic targets.

INTRODUCTION

Excitotoxicity is a pathological cell death process that underpins neuronal cell loss in multiple acute and chronic neurological disorders such as ischemic stroke, Parkinson's and Alzheimer's diseases (reviewed in (Fricker, Tolkovsky, Borutaite, Coleman, & Brown, 2018)). There are no FDA-approved pharmacological agents to protect against excitotoxic neuronal loss in neurological disorders even after decades of intensive studies of the molecular mechanisms underpinning neuronal cell death (Chamorro, Lo, Renu, van Leyen, & Lyden, 2021; Savitz & Fisher, 2007). However, recent findings in a Phase III stroke trial have highlighted putative neuroprotective compounds as a feasible therapeutic option (Hill et al., 2020). As such, further investigations that aim to define the mechanisms of excitotoxic neuronal death are critical to discover therapeutic targets for development of these pharmacological agents (reviewed in (Ballarin & Tymianski, 2018; Fisher & Savitz, 2022)).

Excitotoxicity is initiated by over-stimulation of ionotropic glutamate receptors (iGluRs), especially N-methyl-D-aspartate (NMDA) receptors (Choi, 1988; Olney, 1969; Simon, Swan, Griffiths, & Meldrum, 1984), which permit excessive influx of extracellular calcium (Ca^{2+}) into the cytosol to hyperactivate proteases (Ginet et al., 2014; Lankiewicz et al., 2000; K. K. Wang et al., 1996; Yamashima et al., 1998), neuronal nitric oxide synthase (nNOS) (Sattler et al., 1999) and NADPH oxidase 2 (NOX2) (Brennan et al., 2009). The excitotoxicity-activated proteases cleave specific neuronal proteins to dysregulate their activities, biological functions and stability (Tominaga, Nakanishi, Yasuda, & Yamamoto, 1998; K. K. Wang et al., 1996), thereby contributing to neuronal cell death. Amongst the neuronal proteins dysregulated by excitotoxicity activated proteases are protein kinases and phosphatases, whose proteolytic processing can contribute to neuronal cell death altering the phosphorylation states of specific neuronal proteins (Hossain et al., 2013; Meyer et al., 2014; Shioda, Moriguchi, Shirasaki, & Fukunaga, 2006; J. Wang, Liu, Fu, Wang, & Lu, 2003; Wu et al., 2004). Identification of the proteases, protein kinases and phosphatases activated during excitotoxicity and their substrates in neurons are thus critical for charting the signaling pathways and pathologically-induced cellular events governing excitotoxic neuronal death, and for discovering novel neuroprotective therapeutic approaches (Lipton, 2007).

We previously used mouse cortical neurons, a well-defined *in vitro* model of excitotoxicity to profile excitotoxicity-related changes in phosphorylation of neuronal proteins (Hoque et al., 2019). To gain further insight into post-translational modification events involved in excitotoxic death, the present study sought to identify the substrates of the excitotoxicity-activated proteases and understand how proteolysis alters their biological functions. To do this, we used a quantitative N-terminomics procedure called Terminal Amine Isotopic Labelling of Substrates (TAILS) (Kleifeld et al., 2010) to document changes in stability and the N-termini of neuronal proteins catalyzed by activated proteases during excitotoxicity induced by glutamate over-stimulation. Herein we describe results of our TAILS analysis and illustrate how the results unveil the mechanisms by which the excitotoxicity activated proteases dysregulate key regulators of synaptic organization and functions. Additionally, we demonstrate in a rat model of excitotoxicity that blocking proteolytic processing of a key synapse-enriched protein kinase Src can protect against excitotoxic neuronal loss. Finally, we describe how *in vivo* experiments to validate our TAILS findings led to the discovery of a new mechanism of regulation of calmodulin-dependent protein kinase IIα (CaMKIIα) under both physiological conditions and during excitotoxicity. Since CaMKIIα has been identified as a drug target for protection against excitotoxic neuronal death in an acute neurological disorder (Deng et al., 2017), our discoveries suggest that blockade of proteolytic processing of CaMKIIα and other synaptic protein kinases could be a new neuroprotective strategy to reduce brain damage in neurological disorders.

RESULTS

Remodelling of the neuronal N-terminome occur during excitotoxicity

The signaling pathways directing neuronal death upon over-stimulation of iGluRs remain poorly characterized. While these pathways are likely activated at an early stage following over-stimulation of iGluRs, excitotoxic cell death does not occur immediately; rather it is the prolonged activation of these pathways that causes the ultimate demise of neurons (Hoque et al., 2019; Hossain et al., 2013). One model to study these events is by treating cultured primary mouse cortical neurons with glutamate (reviewed in (Choi, 1990)). Consistent with previous reports, our

experiments involving timed treatment of primary mouse neuronal cultures also demonstrated delayed cell damage and death, observed only after 240 min of glutamate treatment (Figure S1). Therefore, proteomic analysis was performed at the 30-min (early) and 240-min (late) time points after glutamate treatment to identify neuronal proteins demonstrating altered abundance or modification by proteolysis at the early and late stages of excitotoxicity. We reasoned that identifying temporal changes in neuronal proteins undergoing significantly enhanced proteolysis at these two treatment time points could unveil initiating and effector molecular events occurring during excitotoxicity. Some of these events, initiated at the early stage of excitotoxicity when neurons are still alive and sustained until late stages when neuronal death is noticeable, may represent potential drivers of excitotoxic cell death. The TAILS method (Kleifeld et al., 2011), which identifies and quantifies the N-terminal peptides derived from N-termini of cellular proteins, is one of the best approaches to quantitatively monitor changes in the N-termini of neuronal proteins during excitotoxicity. Using this method, we identified and quantified over 5000 N-terminal peptides derived from neuronal proteins in all experimental conditions (Figure 1A, Tables S1A and S2A). Among them, over 70% contain the neo-N-terminal amino acid residues generated by proteolysis of intact neuronal proteins during excitotoxicity (Figure 1A). From the identified neo-N-terminal residues and the abundance changes of the neo-N-terminal peptides, we defined the identities and mechanisms of dysregulation of specific neuronal proteins undergoing proteolytic processing during excitotoxicity.

The two major purposes of proteolysis in cells are (i) to degrade cellular proteins into intermediate peptide fragments destined for clearance into dipeptide and amino acids (herein referred to as degradation) (Figure 1B) and (ii) to process proteins by removing regulatory domains or motifs to form stable truncated protein fragments with altered biological activities (herein referred to as proteolytic processing) (Figure 1C). Degradation of cellular proteins is mediated by proteasomal and lysosomal systems, while proteolytic processing is catalyzed by modulator proteases that specifically target cleavage sites in an intact protein to generate one or more truncated protein fragments. As most of these fragments contain intact functional domain(s), they are relatively stable and may even perform cellular functions different from those of the intact proteins. As shown in Figure 1C, we assigned neo-N-terminal peptides whose abundance was increased as being derived from stable truncated fragments generated from enhanced proteolytic processing of neuronal proteins by excitotoxicity-activated proteases. Conversely, peptides whose

abundance decreased during excitotoxicity were assigned as being derived from neuronal proteins undergoing enhanced degradation for clearance (Figure 1B). Using statistical analysis to define the thresholds for assigning the above groups of neo-N-terminal peptides (Kleifeld et al., 2011; Prudova et al., 2016) (Figures S2A & S2B), we found 234 and 365 peptides underwent significant changes in abundance at 30 min and 240 min of glutamate treatment, respectively, due to enhanced proteolysis of their parent neuronal proteins during excitotoxicity (Figure 2A). These peptides were further classified into those derived from proteins undergoing enhanced proteolytic processing and those derived from proteins undergoing enhanced degradation (Figure 2A; Tables S1B and S2B). These findings reveal for the first time the identities, exact cleavage sites, stability and consequences of proteolysis of cellular proteins targeted by excitotoxicity-activated proteases in neurons.

Among the ~200-300 neo-N-terminal peptides derived from the significantly proteolyzed neuronal proteins during excitotoxicity, only 41 were found in neurons at both treatment time points (Figure S2B), indicating that neuronal proteins undergoing enhanced proteolysis at early stage of excitotoxicity are mostly different from those at late state of excitotoxicity. Additionally, among the 234 identified proteolyzed proteins in, only 77 were proteolytically processed to form stable protein fragments, while the 310 out of 365 of the proteolyzed proteins were proteolytically processed to form stable protein fragments (Figure 2A). Since these protein fragments with neo-N-terminus differ from their parent neuronal proteins in their regulatory properties and/or functions, our results indicate generation of much more dysregulated protein fragments to perturb intracellular signaling in neurons at the late stage of excitotoxicity.

Changes in the neuronal N-terminome during excitotoxicity do not alter protein abundance

To examine whether glutamate-induced changes in neuronal N-terminome led to changes in protein abundance, we performed global proteomic analysis (Figure S3) to identify neuronal proteins and quantify their changes during excitotoxicity (Table S3A). Only 1 and 13 neuronal proteins were deemed to have changed significantly in abundance at 30 and 240 min of glutamate treatment, respectively (Figure S4, Tables S3B and S3C). Thus, in contrast to the extensive changes in the neuronal N-terminome, glutamate treatment for up to 240 min had little impact on neuronal protein abundance. Furthermore, none of the neuronal proteins exhibiting enhanced

proteolysis during excitotoxicity showed significant changes in abundance (i.e. ≥ 2-fold changes) (Figure S5 and Table S4), supporting our prediction that the truncated neuronal fragments generated by proteolytic processing are stable (Figure IB). Intriguingly, none of the neuronal proteins undergoing enhanced degradation during excitotoxicity showed significant decrease in abundance (Figure S5); some even exhibiting a small albeit non-significant increase in abundance. These results suggest that their enhanced degradation is likely a result of their increased turnover i.e. increased biosynthesis and degradation during excitotoxicity.

Calpeptin abolished almost all excitotoxicity-related proteolytic changes in neuronal proteins

Calpeptin is an inhibitor of calpains and cathepsins that has been reported to protect cultured neurons against excitotoxic cell death (W. Wang et al., 2015), suggesting that cleavage of some neuronal proteins by one or both of these proteases contributes to excitotoxic neuronal death. To better understand the roles of these proteases in neuronal death, we used TAILS to compare changes in the N-terminome of neurons treated with glutamate alone or in combination with calpeptin (+Glu and Calpeptin). Using the rationale depicted in Figure 1 to identify neo-N-terminal peptides derived from proteins undergoing significant proteolysis in the co-treated neurons (Figure S6A), we found 16 and 54 neo-N-terminal peptides derived from neuronal proteins undergoing significant proteolysis at 30 and 240 min of the co-treatment, respectively (Figures S6B & S6C). None of these neo-N-terminal peptides were derived from proteins undergoing significant proteolysis at 30 min of glutamate treatment and only two of them were derived from proteins significantly proteolyzed after 240 min of glutamate treatment (Figure S6C, Tables S5, S6 & S7). Hence, calpeptin treatment abolished almost all the proteolytic changes that neuronal proteins undergo during excitotoxicity (Figure S6C), implicating a critical role for calpains and/or cathepsins in catalyzing these events.

Most proteolytically processed proteins in excitotoxic neurons are potential substrates of calpains

The calpain-1 protease core fragment has a deep and narrow active site (Moldoveanu, Campbell, Cuerrier, & Davies, 2004). Hence, to access to this active site, the cleavage site in a

substrate needs to adopt a fully extended conformation and/or reside in an unstructured region located outside a functional domain (Moldoveanu et al., 2004). To identify potential calpain substrates amongst the neuronal proteins with neo-N-terminal peptides derived from enhanced proteolysis in glutamate-treated neurons (Figure 2A), we applied three filtering criteria: (1) the neo-N-terminal peptides are present in neurons treated with glutamate but not in neurons treated with glutamate/calpeptin; (2) the neo-N-terminal peptides were derived from enhanced proteolytic processing of neuronal proteins based on the rationale depicted in Figure 1C and thresholds depicted in Figures S2 and S6; and (3) the neo-N-terminal peptides were derived from cleavage sites located outside a functional domain because proteolytic processing occurs in loop region or unstructured motifs connecting the properly folded functional domains (Figure S7A, Tables S8A and S8B). Using these criteria, 47 and 235 neo-N-terminal peptides respectively, were identified as being derived from proteins potentially cleaved by calpains in neurons at 30 and 240 min of glutamate treatment (Figure 2A). Amongst these were protein kinases such as CaMKIIβ, p21-activated kinase 1, 3 and 6 (PAK1,3 and 6), and the regulatory subunit of protein kinase A (prkara) (Figure S7A). These findings suggest that proteolytic processing by calpains alters signaling events governed by these neuronal protein kinases. In addition, the stable truncated fragments generated by proteolytic processing contain one or more intact functional domains such as the kinase domain, suggesting that some of these fragments retain biological activities and may contribute to the neurotoxic signaling directing cell death during excitotoxicity.

Figure 2B shows the frequencies of amino acids proximal to the identified cleavage sites in neuronal proteins selected by these criteria as potential calpain substrates. The pattern of amino acid preferences from positions P6-P5' of the cleavage site sequences is very similar to that of cleavage site sequences in synthetic peptides cleaved by calpain 1 and calpain 2 *in vitro* (Shinkai-Ouchi et al., 2016) (Figure 2C). Since none of the significantly proteolytically processed proteins exhibited significant reduction in abundance (Figure S5), their cleavage by calpains during excitotoxicity likely generate stable truncated fragments (Table S8).

A protein undergoing degradation for clearance generates numerous unstructured or partially folded intermediate peptide fragments originating from both functional domains and disordered structural motifs. As such, cleavage sites of the degraded proteins do not preferentially reside in unstructured motifs outside a functional domain. Consistent with this prediction, most identified cleavage sites in significantly degraded neuronal proteins were located in functional

domains with well-defined three-dimensional structures (Figure S7B and Table S8). For example, the cleavage sites in Vdac1, Creatine kinase and Pyruvate kinase, (Figure S7B), are not accessible to proteases in the intact proteins. Hence, the neo-N-terminal peptides we identified during excitotoxicity are likely derived from intermediate peptide fragments generated during proteolytic degradation for clearance (Figure S7B). Cathepsins, which catalyze protein degradation are activated during excitotoxicity (reviewed in (Fujikawa, 2015) and (Repnik, Stoka, Turk, & Turk, 2012)). As calpeptin abolished proteolysis of proteins undergoing enhanced degradation in the glutamate-treated neurons (Figure S6C, Tables S5, S6 and S7), it is likely the proteases catalyzing proteolysis of these proteins are cathepsins.

Proteolytic processing events during excitotoxicity significantly impact synaptic organization and function in neurons

Our results indicate that enhanced proteolytic processing in excitotoxic neurons generates stable truncated protein fragments lacking one or more functional domains of the parent protein. As such, these truncated protein fragments may possess dysregulated activities that can perturb biological processes in neurons. To define these processes, we performed Ingenuity Pathway Analysis (IPA) to interrogate how enhanced proteolytic processing of neuronal proteins (listed in Tables S1B and S2B) affects known signaling pathways in cells. This analysis revealed the top-ranked altered signaling pathways during excitotoxicity were those regulating synaptic processes including synaptogenesis, axonal guidance, cell junctions and cell-cell interactions (Figure S8).

We further analyzed how these proteolytically processed neuronal proteins perturb synaptic organization and function using the SynGO and X-link-MS databases which document the locations, functions and protein complex formation of synaptic proteins (Gonzalez-Lozano et al., 2020; Koopmans et al., 2019; Szklarczyk et al., 2019). Our analysis revealed that these proteins mapped to all key synaptic components, with many forming stable protein complexes (Figures 3A and S9). More importantly, they participate in many synaptic biological processes (Figures 3A and S9). Their assignment to specific locations and biological processes of synapses as depicted in Figures 3A and S9 suggests their dysregulation by proteolytic processing and aberrant signaling at synapses contributes to the neurotoxic signaling pathways.

In addition to the predictions by SynGO assignment, twenty neuronal proteins revealed by our TAILS study to undergo enhanced proteolytic processing in excitotoxic neurons were previously found to translocate to post-synaptic density in cortex of neonatal mouse brains following hypoxia-ischemia (Lu et al., 2018; Shao et al., 2017) (Figure 3B). Among them, eight were found to be recruited to the post-synaptic density harboring GluN2B subunit-containing NMDA receptors (Lu et al., 2018) (Figure 3B). Excitotoxicity is a major mechanism directing neuronal loss in hypoxia-ischemia (Choi, 2020) and GluN2B subunit-containing NMDA receptors are NMDA receptors governing excitotoxic neuronal death (Parsons & Raymond, 2014). Based upon these findings, we postulate that these twenty proteins were recruited to the NMDA receptor-containing postsynaptic density during excitotoxicity, where they were proteolytically processed by the over-activated calpains to form stable truncated fragments. For the eight neuronal proteins previously found to be recruited to the GluN2B-containing NMDA receptors in excitotoxic neurons in mouse brain cortex during hypoxia-ischemia (Lu et al., 2018), their proteolytic processing may contribute to the cytotoxic signals emanating from NMDA receptors during excitotoxicity. As such, we selected three protein kinases (Src, DCLK1 and CAMKIIβ) amongst these 8 proteins for further biochemical analysis to illustrate the significance of our TAILS findings because their dysregulation by proteolytic processing could potentially contribute to excitotoxic neuronal death by aberrant phosphorylation of synaptic proteins. We also selected the microtubule-binding protein CRMP2, which is a known regulator of synaptic organization and functions for further biochemical analysis (Wakatsuki, Saitoh, & Araki, 2011).

A new mechanism of dysregulation of the microtubule assembly regulator CRMP2 during excitotoxicity

The synaptic protein CRMP2 (also referred as DPYSL2) is a key regulator of neuronal axon guidance and synaptogenesis (Evsyukova, Plestant, & Anton, 2013) whose dysregulation contributes to neuronal loss in neurodegenerative diseases by an unknown mechanism (Kondo et al., 2019; Wakatsuki et al., 2011). TAILS and Western blot analyses revealed proteolytic processing of CRMP2 to form stable truncated fragments of ~57 kDa (Figures 4A, 4B & S10) during excitotoxicity. Specifically, our TAILS data indicates that CRMP2 was proteolytically processed at sites $A^{516}\downarrow S^{517}$ and $S^{517}\downarrow S^{518}$ in excitotoxic neurons (Figure 4A), leading to the

generation of long truncated N-terminal fragments of ~ 57 kDa and short truncated C-terminal fragments of ~6 kDa. Furthermore, the cleavage sites lie in an unstructured region preferentially targeted by modulator proteases such as calpains (Figure 4C) (Ono, Saido, & Sorimachi, 2016). Accordingly, the cleavage was abolished by calpeptin (Figure S10), suggesting calpains are the upstream proteases catalyzing proteolytic processing of CRMP2 during excitotoxicity.

The C-terminal tail of CRMP2 contains several sites that are sequentially phosphorylated by cyclin-dependent kinase 5 (Cdk5) and glycogen synthase kinase 3β (GSK3β) in neurons (Figure 4D, left panel). In this series of events, phosphorylation of CRMP2 at S522 by Cdk5 (Uchida et al., 2005) directs GSK3β to subsequently phosphorylate T509, T514 and S518 in a processive manner (Uchida et al., 2005). Cleavage at $A^{516}\downarrow S^{517}$ and $S^{517}\downarrow S^{518}$ removes the priming phosphorylation site S522, preventing GSK3β from phosphorylating T509, T514 and S518 in the long, truncated fragment (Figure 4D, right panel). Phosphorylation of these sites impacts the ability of CRMP2 interactions with GTP-bound tubulins (Niwa et al., 2017; Sumi et al., 2018; Wilson, Ki Yeon, Yang, Park, & Khanna, 2014), which is critical for the protein to promote axonal elongation (Inagaki et al., 2001) and modulating microtubule dynamics (Niwa et al., 2017; Yuasa-Kawada et al., 2003).

Figure 4C shows that the long, truncated fragment retains the globular domain critical for promoting microtubule polymerization (Niwa et al., 2017). The microtubule polymerization-promoting activity of CRMP2 is regulated by GSK3β-mediated phosphorylation of these C-terminal tail sites (Yoshimura et al., 2005). Owing to the lack of phosphorylation at these sites, the microtubule polymerization-promoting activity of the fragments cannot be regulated by Cdk5 and GSK3β even though both kinases are known to be aberrantly activated in neurons during excitotoxicity (Chow et al., 2014; Endo, Nito, Kamada, Nishi, & Chan, 2006; Meyer et al., 2014). Consistent with our model, the truncated fragment CRMP2 fragments could not cross-react with the anti-pT509 CRMP2 antibody (Figure 4B). Collectively, the Western blot data validated our TAILS findings and prediction that CRMP2 was cleaved at sites in the C-terminal tail to generate the long-truncated N-terminal fragments that were not phosphorylated by GSK3β at T509. Based on these observations, we also predicted alteration of subcellular localization of the truncated CRMP2 fragments in excitotoxic neurons. Consistent with this prediction, glutamate treatment induced accumulation of neuronal CRMP2 in bead-like structures on dendrites called dendritic blebs (Figure 4E), previously known to form in neurons during excitotoxicity (Greenwood,

Mizielinska, Frenguelli, Harvey, & Connolly, 2007). Moreover, the number of CRMP2-containing dendritic blebs in neurons at 240 min of glutamate treatment was significantly higher than that in neurons at 30 min of treatment (inset of Figure 4E). Since CRMP2 is a crucial regulator of axonal guidance signaling (Inagaki et al., 2001), our findings suggest a mechanism whereby its truncation, reduced phosphorylation at T509, and accumulation in dendritic blebs can potentially contribute to dendritic and synaptic injury associated with excitotoxic neuronal death (Hasbani, Schlief, Fisher, & Goldberg, 2001; Hosie, King, Blizzard, Vickers, & Dickson, 2012).

Excitotoxic neuronal loss is a major contributor to brain damage following ischemic stroke. Given this, we then explored if cleavage of CRMP2 to generate truncated fragments of ~57 kDa also occurs in brain cortex of mice subjected to ischemic stroke (Figure S11A). In agreement with previously published findings (Jiang et al., 2007), C-terminal truncated CRMP2 fragments of ~57 kDa were detectable at 1 – 24h after ischemic stroke induction (Figure S11A), confirming cleavage of CRMP2 to form stable fragments after ischemia stroke.

Proteolytic processing of synapse-enriched protein kinases during excitotoxicity

Several protein kinases are recruited to GluN2B-containing NMDA receptor in neurons in response to hypoxia-ischemia (Lu et al., 2018) (Figure 3B). Among them, DCLK1, Src and CaMKIIβ were of interest as they are known to play critical role in synaptic organization and/or neuronal survival (Ali & Salter, 2001; Deng et al., 2017; Hossain et al., 2013; Shin et al., 2013). As such, they were selected for further *in vitro* and *in vivo* investigations to validate the TAILS findings and to examine if they are potential targets for therapeutic intervention to protect against excitotoxic neuronal loss in neurological disorders.

DCLK1, a regulator of microtubule assembly, axonal guidance and synaptogenesis in neurons (Evsyukova et al., 2013), is a bifunctional protein consisting of two tandem doublecortin (DCX) domains and a C-terminal serine/threonine kinase domain (Gleeson, Lin, Flanagan, & Walsh, 1999; Reiner et al., 2006; Schaar, Kinoshita, & McConnell, 2004; Shu et al., 2006). The tandem DCX domains, which drives microtubule assembly function, are connected to the C-terminal kinase domain by a large PEST sequence (linker rich in proline, glutamic acid, serine and threonine) susceptible to proteolytic cleavage (Patel et al., 2016). Calpains are known to cleave DCLK1 *in vitro* at sites mapped to the PEST motif to generate an N-terminal fragment consisting

of the two DCX domains and a C-terminal fragment consisting of the intact kinase domain and a C-terminal tail (Burgess & Reiner, 2001). Consistent with these previous observations, our TAILS results revealed for the first time enhanced proteolytic processing of DCLK1 during excitotoxicity at the following sites: T^{311}↓S^{312}, S^{312}↓S^{313} and N^{315}↓G^{316} within the PEST sequence (Figure S12A). Cleavage at these sites is expected to generate N-terminal fragments of ~35 kDa conisisting of both DCX domains and C-terminal fragments of ~49 kDa conisisting of the kinase domain and the C-terminal tail. The cleavage was predicted to dysregulate the kinase and microtubule assembly functions of DCLK1 (Burgess & Reiner, 2001) (Patel et al., 2016) (Nawabi et al., 2015). In agreement with the TAILS findings, Western blot of the cell lysates derived from the control and glutamate-treated neurons revealed enhanced formation of truncated DCLK1 fragments of ~50-56 kDa (Figure S12B). As the epitope recognized by the anti-DCLK1 antibody maps to the C-terminal tail, these truncated fragments are predicted to retain the intact protein kinase domain and the C-terminal tail. Besides detecting the 50-56 kDa truncated fragments, the antibody also cross-reacted with several truncated fragments of ~37-45 kDa. These findings suggest that DCLK1 underwent proteolytic processing at multiple other sites in addition to the three cleavage sites identified by our TAILS analysis.

Besides its predicted role as a regulator of the hub domain of NMDA receptor in neurons (Salter & Kalia, 2004) and participation in postsynaptic organization and signaling (Figure 3), Src is also a key contributor to neuronal loss both *in vitro* and *in vivo* (Hossain et al., 2013; D. Z. Liu et al., 2017). We previously demonstrated that Src is cleaved by calpains at a site near its N-terminal region in neurons during excitotoxicity to form a stable truncated fragment ΔNSrc, which acts as a neurotoxic mediator contributing to neuronal death (Hossain et al., 2013). Our TAILS study revealed for the first-time cleavage of Src at F^{63}-G^{64} in glutamate treated neurons (Table S6). The abundance of the dimethyl labelled N-terminal peptide (dimethyl-G^{64}-GFNSSDTVTSPQR^{77}) derived from Src was 5.6-fold higher in the glutamate-treated neurons versus that in the untreated neurons (M/L ratio = 5.6) (Figure 5A, Tables S1B, S4A and S8A), indicating enhanced proteolytic processing of neuronal Src by an excitotoxicity-activated protease catalyzing cleavage of Src at the F^{63}-G^{64} bond. This proteomic finding is validated by the Western blot results (Figure 5A). Second, the cleavage was predicted to generate a stable truncated fragment lacking the N-terminal myristylation domain (also referred to as the SH4 domain) and part of the unique domain (Figure 5B). This prediction was validated by the presence of a truncated fragment ΔNSrc of ~54 kDa at

15 min till 90 min of glutamate treatment in neurons (Figure 5A) (Hossain et al., 2013) and in brain cortex of mice subjected to ischemic stroke (Figure S11B). Furthermore, recombinant Src (R-Src) cleaved by calpain 1 *in vitro* to form a 54 kDa truncated fragment as early as 2 min after incubation (Figure 5C). To determine the cleavage site in R-Src targeted by calpain 1, the reaction mixture consisting of intact R-Src only and that consisting of R-Src and calpain-1 after 120 min of incubation were subjected to isotopic dimethyl labelling prior to tryptic digestion (Figure 5C). A dimethyl labelled peptide identical to the dimethyl labelled neo-N-terminal peptide (dimethyl-G^{64}-GFNSSDTVTSPQR^{77}) detected in the lysate of glutamate-treated neurons, was present only in the R-Src/calpain-1 reaction mixture but not in the reaction mixture with R-Src only (Figure 5C). In summary, these results suggest that calpain 1 or another calpain isoform directly cleaves neuronal Src at the F^{63}↓G^{64} bond during excitotoxicity (Figure 5B).

The two CaM kinase subtypes, CaMKIIα and CaMKIIβ, are both synapse-enriched protein kinases critical to neuronal survival (Buonarati et al., 2020; Kool et al., 2019; Tullis et al., 2021). CaMKIIα and CaMKIIβ are highly homologous and assemble into oligomers of 12 and 14 monomeric subunits, which can consist of both subtypes (Rosenberg et al., 2006). Although much is known about their structures, regulation, and their contribution to neuronal death during excitotoxicity (Bayer & Schulman, 2019; Buonarati, Miller, Coultrap, Bayer, & Reichow, 2021; Guo & Chen, 2022), exactly how they direct excitotoxic neuronal death remains unclear. Our TAILS data revealed proteolytic processing of CaMKIIβ at two cleavage sites: site 1 (M^{282}-H^{283}) in the autoinhibitory and calmodulin binding motif and site 2 (D^{389}-G^{390}) in the linker motif (Figure 6A). Cleavage at sites 1 and 2 is expected to generate stable C-terminal fragments of 28.6 kDa and 17.2 kDa, respectively. Since cleavage at both sites was abolished in the glutamate/calpeptin co-treated neurons and the cleavage sites are located in the autoinhibitory/CaM binding motif and linker motif adopting loop or poorly defined structures (Figures 6A and S7A), they are classified as direct cleavage sites of calpains by criteria depicted in Figure 2A. We next examined whether calpain-1 could cleave recombinant GST-CaMKIIβ *in vitro*. As ischemic stroke induces CaMKIIα in the mouse brain to undergo autophosphorylation at Thr-286 in the autoinhibitory/CaM binding motif (Leurs et al., 2021), we reasoned that CaMKIIβ was also autophosphorylated at the homologous site (Thr-287) in excitotoxic neurons in mouse brains subjected to ischemic stroke treatment. We therefore generated pT287 GST-CaMKIIβ by incubation of GST-CaMKIIβ with Mg^{2+}-ATP in the presence of Ca^{2+}/CaM and examined the cleavage product(s) of calpain-1 derived

from pT287 GST-CaMKIIβ by Western blot analysis. Figure 6B shows that calpain-1 differentially cleaved the unphosphorylated and pT287- GST-CaMKIIβ and generated different C-terminal fragments. The C-terminal fragment of ~25 kDa (C-term. ΔCaMKIIβ fragment-b in Figure 6B) derived from the unphosphorylated GST-CaMKIIβ did not correspond to any one of the two C-terminal fragments predicted from our TAILS data (Figure 6A). Intriguingly, cleavage of pT287-GST-CaMKIIβ by calpain-1 generated a fragment of ~29 kDa (C-term. ΔCaMKIIβ fragment-a) and a fragment of ~17 kDa (C-term. ΔCaMKIIβ fragment-c) (Figure 6B) with molecular masses corresponding to those of the C-terminal fragments generated by cleavage at sites 1 and 2, respectively as predicted by our TAILS data (Figure 6A).

Figure 6C shows that ischemic stroke induced the formation of multiple C-terminal fragments of CaMKIIβ with molecular masses ranging from 26 – 35 kDa. Among them the one of ~29 kDa and marked by a star (Figure 6C) corresponds to C-term. ΔCaMKIIβ fragment-a generated in the *in vitro* experiment (Figure 6B). Taken together, our results from these *in vitro* and *in vivo* experiments support our TAILS findings of cleavage of CaMKIIβ by calpains in neurons during excitotoxicity. Furthermore, autophosphorylation of Thr-287 facilitates calpain cleavage of CaMKIIβ at site 1 (M^{282}-H^{383}) mapped to the autoinhibitory/CaM binding motif (Figure 6B). Since pathological conditions leading to excitotoxic neuronal death induce autophosphorylation of CaMKII (Deng et al., 2017), these conditions are predicted to induce proteolytic processing of CaMKIIβ with site 1 being the preferred cleavage site. In agreement with this prediction, ischemic stroke induced a significant increase in the C-term ΔCaMKIIβ fragment-a.

Blocking calpain-mediated cleavage of neuronal Src protects against excitotoxic neuronal loss

The TAILS and *in vitro* findings showing F^{63}-G^{64} as the calpain cleavage site in Src (Figure 5) are in good agreement with our previous findings that calpains directly cleave Src in a site within its unique domain (Hossain et al., 2013). Based on the sequence surrounding this cleavage site, we designed a cell-permeable peptide TAT-Src consisting of the cell-permeable TAT-sequence and the segment encompassing residues 49-79 in the unique domain of Src and a cell-permeable control peptide TAT-Scrambled (Figure 7A). We then demonstrated that blockade of cleavage of

Src by TAT-Src in excitotoxic neurons (Figure 7A) (Hossain et al., 2013). Importantly, TAT-Src but not TAT-Scrambled could protect the cultured cortical neurons against excitotoxic cell death (Hossain et al., 2013), suggesting TAT-Src as a neuroprotectant *in vitro*.

To explore if TAT-Src can exert neuroprotective action *in vivo*, we first performed stereotaxic infusion of FITC-TAT-Src with a fluorescent tag covalently attached at the N-terminus of TAT-Src, into the cortical and striatal regions of rat brains (Figure 7B). FITC-TAT-Src was detected in neurons but not astrocytes and microglia in the infused regions of the rat brain (Figure 7B) one-hour post infusion, suggesting that it can enter neurons to exert its neuroprotective action. To examine the ability of TAT-Src to protect against excitotoxic neuronal death *in vivo*, TAT-Src, vehicle (water) or TAT-scrambled were stereotaxically injected at four sites in the cortical and striatal regions of rat brains (Figures 7C and 7D). One hour after the injection, neurotoxic dose of NMDA was infused to the same sites to induce excitotoxic brain damage. At 24 h after the infusion of NMDA, the rats were sacrificed, and brain sections were prepared to measure the infarct volume and the number of surviving neurons (Figure 7E). The absence, or reduction in NeuN immunoreactivity, revealed NMDA-induced lesions within the motor and parietal cortex (Figures 7E and 7F). The plot in left panel of Figure 7G shows that total lesion volume was consistent across all treatment groups with no significant difference in the volume of damage detected between groups. Stereological point counting of NeuN positive cells within the lesion revealed treatment-specific effects where the number of neurons in rats treated with TAT-Src was significantly higher than in rats receiving vehicle or scrambled Tat-Src control (Figure 8G, right panel). Thus, injection of TAT-Src prior to NMDA infusion could protect against excitotoxic neuronal loss caused by the injected NMDA. Since FITC-TAT-Src entered neurons but not astrocytes and microglia (Figure 7B), the ability of TAT-Src to protect against neuronal loss in NMDA-induced brain damage is presumably attributed to its blockade of calpain cleavage of neuronal Src to form the neurotoxic truncated Src fragment (ΔNSrc) (Hossain et al., 2013). In conclusion, our results illustrate blockade of pathologically activated proteolytic events as a neuroprotective strategy to reduce brain damage in neurological disorders.

CaMKIIα is differentially processed by calpains in normal and ischemic stroke mouse brains

The *CaMK2b* transcript encoding CaMKIIβ was detectable in embryonic and neonatal mouse brains while *CaMK2a* encoding CaMKIIα was undetectable in these tissues (Bayer, Lohler, Schulman, & Harbers, 1999). As such, CaMKIIβ expression is expected to be much higher than of CaMKIIα in the cultured differentiated embryonic cortical neurons used in our study. The low abundance of CaMKIIα in embryonic brains explains why TAILS analysis of the differential embryonic cortical neurons could detect the neo-N-terminal peptides derived from CaMKIIβ but not those from CaMKIIα (Table S2). Given the high degree of sequence similarity of CaMKIIα and CaMKIIβ (Figure 8A), we predicted that CaMKIIα in adult neurons is also directly cleaved by calpains at the homologous sites 1 and 2 (Figure 8A) to generate two kinase domain-containing N-terminal fragments: CaMKIIα-short and CaMKIIα-long encompassing residues 1 to 282 and 1 to 389 of CaMKIIα, respectively. To validate our prediction, we incubated calpain-1 with unphosphorylated recombinant CaMKIIα (rCaMKIIα) and pT286-rCaMKIIα *in vitro*. Figure 8B shows differential proteolytic processing of unphosphorylated rCaMKIIα and pT286- rCaMKIIα. A fragment with molecular mass (~36 kDa) similar to that of ΔCaMKIIα-long was generated by calpain-1 cleavage of both forms of ΔCaMKIIα, while a fragment with molecular mass (~31 kDa) similar to that of ΔCaMKIIα-short was generated when pT286-rCaMKIIα was cleaved by calpain-1 (Figure 8B). These results suggest that calpain-1 targeted site 2 of both autophosphorylated and unphosphorylated rCaMKIIα. However, site 1 of rCaMKIIα was accessible to calpain-1 only when Thr-286 was autophosphorylated.

Similar to the fragments generated by calpain-1 cleavage of pT286-rCaMKIIα *in vitro*, N-terminal fragments of CaMKIIα with molecular masses similar to ΔCaMKIIα-short (~31 kDa) and ΔCaMKIIα-long (~36 kDa) were detectable in brain cortex of mice subjected to ischemic stroke treatment (Figure 8C, left panel). Ischemic stroke induced an increase in the abundance of ΔCaMKIIα-short but not ΔCaMKIIα-long, suggesting enhanced cleavage of CaMKIIα at site 1 (M^{201}-H^{202}) induced by ischemic stroke. Intriguingly, the ΔCaMKIIα-long exists in brain cortex of both sham-operated mice and mice subjected to ischemic stroke treatment, suggesting that proteolytic processing at site 2 (D^{925}-G^{926}) of CaMKIIα occurred in both physiological and pathological conditions.

To examine if other neuronal CaMKII isoforms including CaMKIIδ and CaMKIIγ were also proteolytically processes by calpains to generate the long and short N-terminal truncated fragments (ΔCaMKII-long and ΔCaMKII-short), we probed the wild type and CaMKIIα knock-

out cortical brain lysates with a pan-CaMKII antibody known to cross-react with all CaMKII isoforms (Figure 8C, right panel and Figure 8D). Since ΔCaMKII-short was detectable in brain cortex of wild type mice but not in CaMKIIα KO mice subjected to ischemic stroke treatment (Figure 8C, right panel), CaMKII-short in wild type ischemic stroke mouse brains were likely mainly derived from cleavage of CaMKIIα at site 1 by calpains.

In summary, these results demonstrate cleavage of CaMKIIα by calpains at site 2 in both physiological and ischemic stroke conditions to generate ΔCaMKIIα-long with intact kinase domain and the autoinhibitory/CaM-binding motif. Upon autophosphorylation at Thr-286 induced *in vivo* by ischemic stroke and *in vitro* by incubation with Mg^{2+}-ATP and CaM, site 1 of CaMKIIα was cleaved by calpains to generate ΔCaMKIIα-short consisting of just the intact kinase domain and a remnant segment of the autoinhibitory/CaM-binding motif.

DISCUSSION

We have for the first time identified over three hundred neuronal proteins associated with synaptic organization and functions that undergo enhanced proteolytic processing to generate stable truncated fragments during excitotoxicity. Since most truncated fragments derived from these proteolytically processed proteins consist of one or more intact functional domains, they likely retain some biological activities of the intact parent neuronal proteins, while other domains are perturbed. Presumably, interplay between these dysregulated truncated fragments alters synaptic organization and functions, which in turn directs neurons to undergo excitotoxic cell death. Hence, these discoveries form a conceptual framework for future investigation to define specific protein-protein interaction networks contributing to neuronal death in excitotoxicity. For example, our findings provided a shortlist of specific pharmacological tools including inhibitors of the proteolytically processed protein kinases and substrate-specific calpain inhibitors such as the neuroprotective TAT-Src peptide (Figure 7) for future investigation to chart signaling pathways orchestrating excitotoxic neuronal death.

One approach to decipher these pathways is through combinatorial phosphoproteomic and N-terminomic analysis of glutamate-treated neurons with and without co-treatment with specific inhibitors of pathologically activated cellular events occurring during excitotoxicity. These include: (i) nerinetide, a cell permeable peptide interfering over-activation of nNOS (Aarts et al.,

2002) and NOX2 (Chen, Brennan-Minnella, Sheth, El-Benna, & Swanson, 2015) by the hyperactivated NMDA receptor (Cook, Teves, & Tymianski, 2012; Sun et al., 2008), (ii) specific inhibitors of the twelve protein kinases dysregulated by proteolytic processing during excitotoxic neurons (listed in Table S8), (iii) specific inhibitors of calpains 1 and 2 (reviewed in (Baudry & Bi, 2016)) and (iv) substrate-specific inhibitors of calpains such as TAT-Src (Figure 7).

We previously demonstrated that ΔNSrc generated by calpain cleavage of Src is a mediator of the neurotoxic signals of the over-stimulated NMDA receptors. Since ΔNSrc is a protein tyrosine kinase, identifying the proteins directly phosphorylated by ΔNSrc in neurons is an appropriate approach to define its neurotoxic mechanism. The proteomic method developed by Bian, *et al.* to define the phosphotyrosine-proteome of cultured cells using the superbinder mutants of SH2 domains (Bian et al., 2016) is therefore a method of choice to identify the substrates of ΔNSrc in neurons during excitotoxicity.

Sequences in proteins proteolytically processed in excitotoxic neurons contain structural features directing their cleavage by calpains

The mechanism of substrate recognition by calpains in cells are poorly understood because of the relative scarcity of confirmed calpain cleavage site data. Since the cleavage sites in the neuronal proteins identified by our TAILS analysis were the exact sites targeted by calpains in neurons, they therefore represent genuine cleavage sites of calpain substrates *in vivo*. Our data demonstrates that in excitotoxic neurons, the pattern of amino acid preferences from positions P6-P5'of the cleavage site sequences in neuronal proteins proteolytically processed by calpains is very similar to that in synthetic peptides cleaved by calpain 1 and calpain 2 *in vitro* (Figure 2). These findings suggest that the active site and substrate-binding sites (exosites) of calpains have specific structural features in P6-P5' of the cleavage site sequences in their *in vivo* substrates.

duVerle and Mamitsuka documented around 100 experimentally confirmed calpain cleavage sequences in mammalian proteins (duVerle & Mamitsuka, 2019). Among them, the exact sites of calpain cleavage sites were determined by *in vitro* studies. As such, it remains unclear if the cleavage sites they determined correspond to the sites of cleavage in these proteins by calpains *in vivo*. Based upon the limited data of calpain cleavage sites in protein substrates and results of peptide library studies to define the optimal cleavage sequences (Cuerrier, Moldoveanu, & Davies,

2005; Shinkai-Ouchi et al., 2016), a number of algorithms for prediction of calpain substrates and the cleavage sites were designed. The most notable algorithms include calCleaveMKL (duVerle & Mamitsuka, 2019), iProt-Sub (Song et al., 2019) , DeepCalpain (Z. X. Liu et al., 2019) and GPS-CCD (Z. Liu et al., 2011). Here, we demonstrated for the first time a high degree of conformity of amino acid preferences at the P6-P5' positions in both the potential calpain substrates in neurons and the *in vitro* peptide substrates of calpains 1 and 2, which are the major calpain isoforms expressed in neurons (Figures 2B and 2C). Of the 200-300 cleavage sites in neuronal proteins potentially cleaved by calpains during excitotoxicity identified in our study (Figure 2), over 90% were identified for the first time as potential calpain cleavage sites in properly folded proteins in live cells. As such, incorporating information of these newly identified cleavage site sequences and/or three-dimensional structures of the corresponding calpain substrates will improve the predictive accuracy of these algorithms.

Besides conformity of the primary structure proximal to the cleavage site with the optimal calpain cleavage sequence and the three-dimensional structural features of a potential calpain substrate revealed in our study, co-localization of the calpain substrate with a specific isoform of calpains also governs whether it is proteolytically processed to form stable truncated fragments *in vivo*. For example, the C-terminal tail of calpains 1 and 2 contains different PDZ-binding motifs which target them to different subcellular compartments where they proteolyze specific subsets of protein substrates (Baudry & Bi, 2016; Y. Wang, Briz, Chishti, Bi, & Baudry, 2013). Future investigations to decipher where and when the potential calpain substrates identified in our TAILS analysis form protein complexes with calpains 1 and 2 in neurons during excitotoxicity will further bridge the knowledge gap concerning how the two isoforms of calpains recognize their substrates in neurons.

Neuronal proteins proteolytically processed during excitotoxicity are potential targets for the development of neuroprotective therapeutics

Currently, there is no FDA-approved neuroprotective drug for treating patients suffering from acute neurological disorders or neurodegenerative disease. This pessimistic scenario has been challenged by the promising results of two clinical trials of a cell membrane permeable peptide nerinetide, which inhibits a key pathological event directing excitotoxic neuronal death – binding of the scaffolding protein PSD95 to the NMDA receptor (Aarts et al., 2002; Hill et al., 2020; Hill

et al., 2012). The positive clinical outcomes of nerinetide treatment illustrates that other cellular events occurring in neurons as a result of excitotoxicity are potential therapeutic targets for the development of neuroprotective strategies for the treatment of ischemic stroke patients. Proteolytic processing of Src to generate the neurotoxic truncated fragment ΔNSrc is also a pathological event directing neuronal death (Hossain et al., 2013) and we demonstrated the substrate-specific calpain inhibitor Tat-Src could protect against neuronal cell loss *in vivo* (Figure 7), small-molecule compounds mimicking TAT-Src peptide in specifically blocking calpain cleavage of Src in neurons (Figure 7) are potential neuroprotective drug candidates to reduce excitotoxic neuronal loss in neurological disorders.

It is noteworthy that not all substrate-specific cell membrane-permeable peptides blocking neuronal proteins from being proteolytically processed by calpains are potential neuroprotectants. For example, cell-permeable peptide inhibitors that specifically block calpain cleavage of CaMKIIα and CaMKIIβ at sites 1 and 2 (Figure 8) are not suitable for use as neuroprotective therapeutics. Cleavage site 1 (M^{282}-H^{283} of CaMKIIβ) is located within the autoinhibitory/CaM-binding motif. Hence, even if a cell-permeable peptide derived from the sequence around this cleavage site can specifically block calpain cleavage of CaMKIIβ in excitotoxic neurons, it would not be suitable for use as a neuroprotectant, as the peptide sequence contains the autoinhibitory/CaM-binding motif, which can bind CaM and interfere with the physiological function of CaM *in vivo*. Thus, careful peptide sequence optimization to eliminate its CaM-binding ability would be needed. Since autophosphorylation of CaMKIIα at Thr-286 impairs its CaM-binding activity, replacing Thr-286 in the peptide sequence with a phosphomimetic amino acid may achieve this aim. For site 2 (D^{389}-G^{390} of CaMKIIβ), proteolytic processing of CaMKIIβ and CaMKIIα at this site occurs in both sham-operated and ischemic stroke mouse brains (Figure 8), indicating that it is a proteolytic processing event occurring in both physiological and pathological conditions. Hence, the cell-permeable peptide derived from the sequence around this site is not suitable for use a neuroprotective therapeutic because it can potentially interfere with modifications of CaMKIIα and CaMKIIβ by calpains under physiological conditions. It is thus necessary to define the effects of blockade of calpain cleavage of the proteolytically processed neuronal proteins identified in our TAILS analysis before they are chosen as the targets for future development of neuroprotective therapeutics. Nonetheless, besides identifying calpain cleavage of Src as a potential target for development of neuroprotective therapeutics, the proteolytic processing

events during excitotoxicity constructed by our TAILS analysis also provide the conceptual framework for identifying other calpain substrates as potential targets for neuroprotective therapeutics development.

Calpain-catalyzed proteolytic processing as a physiological and pathological regulatory mechanism of neuronal CaMKII

Results of Western blot analysis indicated that cleavage of CaMKIIα at site 2, leading to the formation of ΔCaMKIIα-long consisting of the intact kinase domain and the autoinhibitory/CaM-binding motif, occurred in both sham-operated and ischemic stroke mouse brains (Figures 8C, 8D and 8E), suggesting proteolytic processing as a physiological regulatory mechanism of CaMKII. In contrast, ΔCaMKII-short, consisting of just the intact kinase domain was generated by cleavage of CaMKIIα and other neuronal CaMKII isoforms at site 1 was generated in ischemic stroke mouse brains only (Figures 8C, 8D and 8E). Hence, proteolytic processing of CaMKIIα and other isoforms at site 1 leading to the formation of ΔCaMKII-short is a pathological regulatory mechanism of CaMKII.

Autophosphorylation at Thr-286 of CaMKIIα and the homologous threonine residue in other CaMKII isoforms allows CaMKII to remain active without stimulation by Ca^{2+}/CaM (Bhattacharyya, Karandur, & Kuriyan, 2020; Miller & Kennedy, 1986). As Thr-286 and the homologous threonine residues in CaMKII isoforms are located in the autoinhibitory/CaM-binding motif, suggesting that its phosphorylation can affect the accessibility of both cleavage sites 1 and 2 to calpains. Results of *in vitro* analysis revealed that cleavage at both sites occurred only when Thr-286 and Thr-287 of CaMKIIα and CaMKIIβ, respectively were autophosphorylated (Figures 6B and 8B). This effect of phosphorylation at Thr-286/Thr-287 on calpain-catalyzed proteolysis of CaMKIIα and CaMKIIβ was in agreement with results of the *in vitro* studies reported by Rich, *et al.* (Rich, Schworer, Colbran, & Soderling, 1990) and Kwiatkowski and King (Kwiatkowski & King, 1989). These findings suggest that autophosphorylation at Thr-286/Thr-287 is a pre-requisite for calpain-mediated cleavage of CaMKII at both sites 1 and 2.

Besides enhanced proteolytic processing by calpain cleavage at site 1, CaMKIIα and its isoforms including CaMKIIβ and CaMKIIδ expressed in neurons (referred to as CaMKIIs) undergo significant autophosphorylation at Thr-286. Upon phosphorylation of Thr-286 and its homologous threonine, CaMKIIs exhibit autonomous Ca^{2+}/CaM-independent activity. How might

autophosphorylation at Thr-286 and calpain cleavage at site 2 contribute to excitotoxic neuronal death and brain damage in ischemic stroke? Using the mouse model of cardiac arrest and pulmonary resuscitation (CA/CPR) that cause excitotoxic neuronal loss, CA/CPR induced significant brain damage and a significant increase in autophosphorylation at Thr-286 and the homologous threonine of CaMKII and other isoforms in synaptosome membrane fractions (Deng et al., 2017). Treatment with the tight binding CaMKII inhibitor tatCN19o at 30 min after CA/PCR reduced autonomous CaMKII activity and reduced the brain damage inflicted by the treatment, suggesting that the neuroprotective action of tatCN19o is attributed to its inhibition of autonomous kinase activity and/or autophosphorylation at Thr-286 of CaMKII. Further investigation with the transgenic mice expressing the phosphorylation-deficient T286A-CaMKII mutant revealed that, similar to the effects of tatCN19o, CA/CPR inflicted much less brain damage. In summary, these findings confirm the neurotoxic role of sustained Ca^{2+}/CaM-independent activation of CaMKIIs as a result of autophosphorylation at Thr-286 and the homologous threonine residues. In light of our TAILS and biochemical findings (Figures 6 and 8), we hypothesize that CaMKIIs autophosphorylated at Thr-286 and homologous threonine residues in excitotoxic neurons are cleaved by calpains at site 1, leading to the formation of the constitutively active ΔCaMKII-short, which phosphorylates specific neuronal proteins to direct neuronal death (see model in Figure 8E). Future investigation into the effects of recombinant ΔCaMKII-short on neuronal survival will reveal whether ΔCaMKII-short is a mediator of excitotoxic neuronal death. Of relevance, we previously demonstrated that the truncated fragment ΔNSrc generated by proteolytic processing of Src was a mediator of excitotoxic neuronal death (Hossain et al., 2013). Additionally, a recombinant truncated CaMKII fragment with an intact kinase domain was highly active and its expression in neurons induces AMPA receptor activation in synapses (Hayashi et al., 2000), confirming the ability of truncated fragment of CaMKII to induce aberrant signaling events in neurons.

What are the physiological consequences of calpain cleavage of CaMKIIs at site 2 to generate ΔCaMKII-long? Since the CaMKII-long fragments consisting of the intact kinase domain and the autoinhibitory/CaM-binding motif, its activity is still under the control of Ca^{2+}/CaM. However, lack of the hub domain allows CaMKII-long to dissociate from the CaMKII oligomeric complexes and translocate and phosphorylate neuronal proteins in a different subcellular location.

Future investigations to identify the substrates and binding partners of CaMKII-long in neurons will shed light on its potential physiological functions.

MATERIALS AND METHODS

Experimental Design

Animals

Both mice (C57BL/6) and rats (male, male Hooded Wistar) were used in both the *in vitro* and *in vivo* studies. For preparation of cultured mouse cortical neurons, the procedures were approved by the University of Melbourne Animal Ethics Committee (License number: 161394.1) and were performed in accordance with the Prevention of Cruelty to Animals Act 1986 under the guidelines of the National Health and Medical Research Council Code of Practice for the Care and Use of Animals for Experimental Purposes in Australia. Briefly, embryos were collected from pregnant C57BL/6 mice (gestational day 14-15) after they were euthanized by CO_2 asphyxiation.

Brains from sham-operated mice and those from mice subjected to ischemic stroke and traumatic brain injury were prepared solely for the construction of spectral libraries. All experiments were performed in strict accordance with the guidelines of the National Health & Medical Research Council of Australia Code of Practice for the Care and use of Animals for Experimental Purposes in Australia. For the dual carotid artery ligation stroke (ischemic stroke) mouse model and the controlled cortical impact mouse model of traumatic brain injury (TBI), C57Bl/6 mice (20-30g), male, were used.

For the animals used in the rat model of neurotoxicity, male Hooded Wistar rats weighing 300-340g sourced from Laboratory Animal Services, University of Adelaide, Australia were used. The protocol was approved by the St Vincent's Hospital animal ethics committee (AEC016/12). All surgery was performed under general anesthesia, and paracetamol (2 mg/kg in drinking water) was provided for 24 h prior to and after surgery in order to minimize suffering and included monitoring each rat throughout the length of the study to ensure their wellbeing.

For the animals used in the mouse photothrombotic stroke models, young male C57BL/6*J* (3-4 months, 27-30 g) were obtained from the Biomedical Research Facility, University of Otago, New Zealand. *Camk2a*$^{-/-}$ mice (*Camk2*^{atm3Sva}, MGI:2389262) mice backcrossed into the

C57BL/6*J* background were bread in the *In Vivo* Pharmacology Research Unit, University of Copenhagen, Denmark. All procedures on wildtype C57BL/6*J* mice were performed in accordance with the guidelines on the care and use of laboratory animals set out by the University of Otago, Animal Research Committee and the Guide for Care and Use of Laboratory Animals (NIH Publication No. 85–23, 1996). For stroke surgeries involving *Camk2a*$^{-/-}$ mice ethical permission was granted by the Danish Animal Experiments Inspectorate (permission 2017-15-0201-01248), and all animal procedures were performed in compliance with Directive 2010/63/EU of the European Parliament and of the Council, and with Danish Law and Order regulating animal experiments (LBK no. 253, 08/03/2013 and BEK no. 88, 30/01/2013). All procedures were performed in accordance with the ARRIVE (Animal Research: Reporting In Vivo Experiments) guidelines. All measures were taken to minimize pain, including subcutaneously administration of buprenorphine hydrochloride (0.1 mL of a 0.5 mg/kg solution, Temgesic®) as pre-emptive post-surgical pain relief.

Experimental Model I - Preparation of cultured mouse primary cortical neurons

Cultured mouse cortical neurons were prepared for the construction of spectral libraries, multi-dimensional proteomic analyses and validation of the proteomic results by biochemical methods. The cortical region was aseptically micro-dissected out of the brains of the embryos, free of meninges and digested with 0.025 % (w/v) trypsin in Krebs Buffer (0.126 M NaCl, 2.5 mM KCl, 25 mM $NaHCO_3$, 1.2 mM NaH_2PO_4, 1.2 mM $MgCl_2$, 2.5 mM $CaCl_2$, pH 7.2) and incubated at 37°C with shaking to dissociate the connective tissues. After 20 min of incubation, 0.008% (w/v) DNase I (Roche Applied Science) and 0.026 % (w/v) soybean trypsin inhibitor (Sigma) in 10 ml Krebs solution (DNase I/soybean trypsin inhibitor solution) were added to the suspension to stop the trypsin action and initiate digestion of DNA. Gentle mixing by inversion of the suspension was performed. Cells in the suspension were collected by centrifugation at 1000 × g for 3 min at room temperature. They were resuspended in 1 ml of DNase I/soybean trypsin inhibitor solution. After aspiration of the supernatant, the cells were resuspended in plating medium (minimum essential medium (MEM) supplemented with 2 mM L-glutamine, 0.22% v/v NaHCO3, 1% penicillin-streptomycin, 5% v/v horse serum and 10% v/v fetal calf serum). Approximately 800,000 cells per well were seeded to a 12-well plate pre-treated with 0.1 mg/ml Poly-D-lysine. After incubation at 37°C in 5% CO_2 for 2 h, the medium was replaced with

neurobasal medium supplemented with 0.2 mM L-glutamine, 0.01 mg/ml penicillin-streptomycin and B27 supplement (NB/B27). Cultures were maintained for seven days (days *in vitro* 7 (DIV7)). Immunofluorescence microscopy analysis using antibodies against neuronal, astrocytic and microglial markers revealed that the DIV7 culture contained 94.1 ± 1.1% neurons, 4.9 ± 1.1% astrocytes, <1% microglia and <1% other cells (data not shown). The DIV7 cultures, highly enriched with neurons, were used for the experiments.

To induce excitotoxicity, the DIV 7 neuronal cultures were treated with 100 μM glutamate in NB/B27 for 30 and 240 min. For co-treatment with glutamate and calpeptin, the DIV 7 neuronal cultures were treated with 100 μM glutamate and 20 μM calpeptin in NB/B27 for 30 and 240 min. For control, viable untreated cells from the same batch of DIV 7 neuronal cultures were used for proteomic and biochemical analyses.

Experimental Model 2 - Mouse models of ischemic stroke used for proteomic and biochemical analyses

The dual carotid artery ligation (DCAL) ischemic stroke mouse model was used for proteomic analysis while the focal photothrombotic ischemic stroke mouse model was used for the biochemical investigation of proteolytic processing of CaMKII, SRc and CRMP2 *in vivo*. To generate the DCAL stroke model, mice were placed into a plastic box and initially anaesthetized with 5% Isoflurane (in 1.0 ml/min O_2), and maintained on 1.5% Isoflurane for the duration of the experiment. A temperature probe connected to a thermoblanket (Harvard Apparatus Ltd., Kent, UK) was inserted into the rectum to monitor body temperature, and body temperature was maintained at 37°C throughout the experiment using a heat lamp. All surgical procedures were performed using aseptic technique. Surgical instruments were sterilized using a bead sterilizer (Steri350, Sigma Aldrich) prior to use. The mouse was affixed in a supine position on the thermoblanket using tape, and the neck shaved and swabbed with alcohol. Through a ventral midline incision, the carotid arteries were exposed via blunt dissection and carefully dissected clear of the vagus nerve and surrounding tissue. A stabilization period of 10 min is allowed between the isolation of each artery. The right jugular vein was also exposed via a cut to the skin and blunt dissection for the purpose of drug administration. Following the surgical procedures, the animals were allowed to stabilize for 10 min before the experiment proceeded. The left carotid artery is permanently ligated using 6-0 silk suture (6-0 black braided silk suture, SDR Scientific, Sydney,

Australia). Following a stabilization period of 10 min, the right carotid artery is then transiently occluded for 30 min using a small hemostatic clamp. After the transient occlusion, the neck incision was closed using tissue glue (Leukosan Adhesive, BSN medical Inc.), and the mouse allowed to recover under 1% O_2. Animals were housed separately following surgery with access to food and water *ad libitum*. At 24 h post-surgery, the mice were euthanized, and their brains removed and stored at -80 ºC.

For the mouse model of photothrombotic stroke used for biochemical investigation of proteolytic processing of CaMKII, Src and CRMP2, young adult male C57BL/6J mice (3-4 months, 27-30 g, n = 4-5) were subjected to photothrombotic stroke as previously described (Clarkson, Huang, Macisaac, Mody, & Carmichael, 2010). In brief, mice were anesthetized with isoflurane (4% induction, 2-2.5% maintenance in O2) and body temperature was kept at 37 °C using a heating pad throughout the procedure. Mice were placed in a stereotactic frame (9000RR-B-U, KOPF; CA, USA). The skin was sterilized using chlorhexidine (30% in 70% ethanol, Hibitane®). Following exposure of the skull through a midline incision, it was cleared of connective tissue and dried. A cold light source (KL1500 LCD, Zeiss, Auckland, New Zealand) attached to a 40x objective providing a 2-mm diameter illumination was positioned 1.5 mm lateral from bregma. Next, 0.2 mL of Rose Bengal (Sigma-Aldrich, Auckland, New Zealand; 10 mg/mL in normal saline) was administered i.p 5 min prior to illumination. Then, the brain was illuminated through the exposed intact skull for 15 minutes with 3300 K color temperature intensity. The skin was glued and animal were returned to their home a cage placed on a heating pad during the wake-up phase. Sham surgery was performed in the exact same way, except that saline was injected instead of Rose Bengal. Mice were housed in groups of two to five under standard conditions in individually ventilated cages (IVC: Tecniplast): 21 ± 2 °C and humidity of 50 ± 10%, on a 12 h light/dark cycle with ad libitum access to food and water. Mice were monitored and weighed after surgery. All animals were randomly assigned to experimental groups. No deaths were reported during these studies. One mouse was excluded from stroke + 4 h survival group due to the lack of any visible stroke being detected, most likely due to experimenter error with the Rose Bengal most likely being injected into the bladder. Mice were euthanized by cervical dislocation, followed by rapid extraction of the brain at 1, 3, 4, 6, 12 and 24 h after stroke induction. Brains were snap-frozen and stored at -80 °C until further processing.

A mouse model of traumatic brain injury (TBI) was used to generate brain lysates to construct the spectral libraries for global proteomic analysis. For this model, controlled cortical impact (CCI) was induced. This procedure is well established and induces a reproducible brain trauma with a mortality of less than 5% (Sashindranath et al., 2011). After anesthesia with 0.5 g/kg avertin (1.875% solution dissolved in 0.9% sodium chloride pre-warmed at 37ºC, 2,2,2-tribromoethanol; Sigma Aldrich #T48402; 1mg/ml in tert-amyl alcohol), injected intra-peritoneally (i.p.), mice were placed in a stereotaxic frame (Kopf, Tujunga, CA). A sagittal incision in the midline of the head was performed and the skull cleaned with a 6% hydrogen peroxide solution using a sterile cotton swab. This was followed by a 5 mm diameter craniotomy performed with a drill over the left parietal cortex. The impactor was positioned in a 20º angle with the tip (cylindrical rod) touching the brain surface, and a single blunt force trauma was inflicted to the exposed brain area with an impact depth of 2mm, a velocity of 5 m/s and dwell time of 400 ms inducing a moderate to severe brain trauma. The exposed brain was then sealed using bone wax (Ethicon, Johnson and Johnson #W810T) and the skin incision was sutured with a non-absorbable braided treated silk (Dynek, Dysilk) and treated with a local anesthetic (xylocaine) and an antiseptic (betadine). For the sham procedure, only the scalp incision, without craniotomy and CCI was performed since even the craniotomy without CCI results in a brain lesion (Sashindranath, Daglas, & Medcalf, 2015). Regardless of the experimental design, however, mice were placed on a 37 ºC heat pad within 30 min after induction of anesthesia for post-surgery recovery, and they usually recovered within 40-60 min. Animals were housed separately following surgery with access to food and water *ad libitum*. At 24 h post-surgery, the mice were euthanized, and their brains removed and stored at -80 ºC.

To prepare the brain lysates from DCAL ischemic stroke mice, TBI mice and sham-operated mice for generation of the spectral libraries, we homogenized the frozen tissue biopsies in ice-cold RIPA buffer (50 mM Tris-HCl, pH 7.0, 1 mM EDTA, 5 mM EGTA, 1 mM dithiothreotol, 10% (v/v) glycerol, 1 % Triton X-100, 0.01% SDS, 150 mM NaCl, 50 mM NaF, 40 mM sodium pyrophosphate, 0.5 mM Na_3VO_4, 50 mM β-glycerol phosphate, 0.2 mM benzamidine, 0.1 mg/ml phenylmethyl sulfonyl fluoride (PMSF)) supplemented with 1% cOmpleteTM protease inhibitor cocktail (Roche Diagnostics). The tissue lysates were harvested and centrifuged at 12500×g for 15 min at 4 ºC. Supernatants were collected and the protein

concentrations were determined by BCA protein assay (Pierce-Thermo Scientific) prior to storage at -80 ºC for further processing.

For preparation of the brain lysate from photothrombotic ischemic mice, brains were processed and prepared for Western blot analysis as previously described in Leurs *et al* (Leurs et al., 2021). In brief, peri-infarct tissue was collected at - 20 °C using a tissue punch, and tissue homogenization was performed using a Bullet Blender in RIPA buffer supplemented with 1% cOmpleteTM protease inhibitor cocktail (Roche Diagnostics), 1% phosphatase inhibitor cocktail 2 (#P5726, Sigma-Aldrich) and 1% phosphatase inhibitor cocktail 3 (#P0044, Sigma-Aldrich). Protein concentration was determined with the Pierce™ BCA Protein Assay Kit (#23227, Thermo Fisher Scientific). Samples were prepared for Western blot analysis by addition of 4x Fluorescent Compatible Sample Buffer (#LC2570, Thermo Fisher) and 100 mM DTT with a protein concentration of 2 µg/µL. Samples were heated for 5 min at 95 °C, sonicated and centrifuged 11,000 x g for 2 min at 4 °C. 20 µg sample were loaded onto 4-20% Mini-PROTEAN® TGXTM gels (Bio-Rad), and SDS-PAGE was performed for 40 min (200 V) with 1x Tris/glycine/SDS (25 mM Tris, 192 mM glycine, 0.1% SDS, pH 8.3) running buffer. Protein transfer to a PVDF membrane (#4561096, Biorad) was performed using the Trans-Blot® TurboTM transfer system (Bio-Rad) (2.5A, 7min), and membranes were blocked 1x BlockerTM FL Fluorescent Blocking Buffer (#37565, Thermo Fisher) for 30 min at room temperature.

Following primary antibody incubation, membranes were washed 3x 5 min washes in 1x tris-buffered saline (TBS) with 0.1% Tween-20 detergent (TBS-T). Next, membranes were probed with species-specific secondary antibodies, and washed again 3x for 10 min with TBS-T. Image were aquired with the iBright FL1500 imaging system (Invitrogen), and signals were quantified in Image Studio (Lite version 5.2). Data was analyzed in GraphPad Prism (version 8), presented as mean ± SD, and statistical analysis was performed using One-way ANOVA, post-hoc Dunnett's test.

Experimental Model 3 - in vivo model of NMDA neurotoxicity

To induce NMDA excitotoxicity *in vivo*, male hooded Wistar rats (n = 12) weighing 300-340g (Laboratory Animal Services, University of Adelaide, Australia) were used. Rats were anesthetized with intraperitoneal administration of ketamine and xylazine (75mg/kg and 10 mg/kg, respectively), and maintained by inhalation of isoflurane (95% oxygen and 5% isoflurane). Rats

were positioned in a stereotaxic frame (Kopf), and 4 burr holes were drilled into the right hemisphere corresponding to the predetermined sites for NMDA infusion (Site 1: AP +3.2, ML -2.7, DV -2.9; Site 2: AP +2.4, ML -2.7, DV -2.9; Site 3: AP +0.6, ML -3.8, DV -2.9; Site 4: AP +0.12, ML -2.8, DV -5.9). Rats were randomly assigned into 3 cohorts and received either vehicle (sterile Milli-Q H_2O, 3 µl per site), TAT-SRC peptide (5 mM in sterile MilliQ H_2O, 3 µl per site), or TAT-Scrambled peptide (5 mM in sterile MilliQ H_2O, 3 µl per site) via direct infusion at 0.2 µl/min into each site 1 h prior to infusion of NMDA (70 mM, 1µl PBS per site). Following infusion each burr hole was filled with bone wax and wounds sutured. In separate studies, rats were infused with FITC-TAT-SRC peptide without NMDA to assess neuronal uptake and cell specificity at one hour after infusion.

Rats that received treatment with NMDA +/- Tat-Src, Tat-Scrambled or Vehicle were allowed to recover for 24 h prior to lethal overdose (lethobarb) and decapitation. Forebrains were collected and rapidly frozen over liquid nitrogen and stored at -80°C prior to processing. Coronal sections (16 µm thick) were prepared using a Leica cryostat (Leica Microsystems, Wetzlar, Germany) across the 4 coronal planes corresponding to the NMDA infusion sites.

For immunohistochemistry analysis, immunofluorescence staining was performed in forebrain tissue sections to identify Tat-Src cell specificity and treatment effects following NMDA excitotoxicity. Sections were first fixed in 4% PFA for 15 minutes at RT prior to wash (3 × 5 min washes with 0.1 M PBS) and a blocking step in 5 % NGS and 0.3 % Triton X-100 and 0.1 M PBS for 30 min. Sections were again washed (3 × 5 min washes with 0.1 M PBS) and adjacent sections incubated with primary antibodies to detect neurons, astrocytes and microglia using the following primary antibodies: mouse anti-NeuN (1:500, Chemicon); mouse anti-GFAP (1:400, Millipore); and mouse anti-OX-42 (1:100, Serotec) in 2% NGS, 0.3% Triton X-100 and 0.1M PBS overnight at 4°C. The following day sections were again washed (3 × 5 min washes with 0.1 M PBS) and incubated with secondary fluorophore-conjugated antibody Alexa 555 goat anti-mouse (1:500, Thermo Fisher Scientific) for visualization of each primary antibody. For all experiments, DNA counterstain DAPI (Molecular Probes, Thermo Fisher Scientific) was applied before coverslipping with ProLong gold anti-fade reagent (Invitrogen). Control studies included omission of each primary antibody.

For lesion assessment and stereology of rat brains, triplicate sections from each NMDA infusion site were visualized using an Olympus microscope (Albertslund, Denmark) equipped with

a 578–603 nm filter set for the detection of red fluorescence, at ×20 magnification. NMDA-induced lesions were identified by a distinct reduction or absence of NeuN fluorescence, which was analysed manually by tracing the site of injury using ImageJ software (NIH, Bethesda, MD, USA). Lesion volume was then determined as described by Osborne, *et al*. by integrating the cross-sectional area of damage between each stereotaxic infusion site and the distance between sites (Osborne et al., 1987). The number of NeuN positive cells within each lesion were also point counted using ImageJ software using a grid overlay to estimate the total number of NeuN positive cells within each region, and expressed as number of cells/mm^2. Data obtained for infarct volume and the effects of treatment on neuronal counts were analysed by one-way ANOVA followed by the Bonferroni post-hoc test. Data were analysed using GraphPad Prism, version 6 (GraphPad Software Inc., San Diego) and presented as mean ± standard error of the mean (SEM). Statistical significance was defined as $p < 0.05$.

For investigation of cell specificity of TAT-Src peptide in rat brains, Immunofluorescence within adjacent tissue sections was visualized using a fluorescent microscope equipped with a 578–603 nm filter set for detection of red fluorescence (NeuN, GFAP, OX-42), a 495–519 nm filter set for the detection of green fluorescence (FITC-Tat-Src), and a 478-495nm filter set for detection of blue fluorescence (DAPI) (ZeissAxioskop2, North Ryde, Australia). Immunohistochemical co-localization of the stereotaxically infused FITC-Tat-Src was clearly identified in the cortex and striatum and was co-localized with the neuronal marker NeuN but not with the astrocytic marker GFAP or the microglial marker OX-42 one-hour post-infusion.

For infarct assessment, absence or reduction in NeuN immunoreactivity in brain sections was monitored because it revealed NMDA-induced lesions within the motor and parietal cortex as well as the striatum. Total lesion volume was consistent across treatment groups with no significant difference in volume of damage detected between groups ($P > 0.05$, n=3/group, one-way ANOVA). Stereological point counting of NeuN positive cells within the lesion revealed treatment specific effects where the number of neurons in rats treated with TAT-Src was significantly greater than in rats receiving vehicle or scrambled Tat-Src control ($P < 0.0001$, n=3/group, one-way ANOVA).

MTT cell viability assay and LDH release assay of neuronal death

Primary cortical neurons were incubated for 480 min with and without the addition of 100 μM of glutamate. The control neurons were incubated for 480 min in culture medium. For neurons

treated with glutamate for 30 min, 60 min, 120 min and 240 min, they were pre-incubated in culture medium for 450 min, 420 min, 360 min and 240 min, respectively prior to the addition of glutamate to induce excitotoxicity. For neurons treated with glutamate for 480 min, they were treated with glutamate without pre-incubation in culture medium.

Cell viability was determined from primary cortical neurons (seeded in 24-well plates) using the 3-(4,5-dimethylthiazole-2-yl)-2,5-diphenyltetrazolium bromide (MTT) assay. MTT stock solution (5 mg/ml (w/v) in sterile PBS) was diluted 1/100 in culture medium. At the end of treatment of cultured neurons, the culture medium was aspirated and replaced by the diluted MTT solution. After incubation for 2 h, the diluted MTT solution was removed and 200 µl DMSO was added per well to dissolve the formazan crystals formed. Absorbance at 570 nm was measured using the Clariostar Monochromator Microplate Reader (BMG Lab Technologies, Durham, NC). Cell viability was expressed as a percentage of the control cells.

The activity of LDH released from the damaged neurons to the culture medium was measured. Briefly, 50 µl of culture medium from each well of the culture plate was transferred to 96 well-microtiter plates (Falcon). 100 µl of LDH assay mixture containing equal volume of LDH assay substrate solution, LDH Assay dye solution and LDH assay cofactor was then added to each well. The reaction was allowed to proceed at room temperature for 30 min in the dark and was stopped by adding 50 µl of 1 mM acetic acid. The absorbance at 490 nm of whole mixture was measured in triplicate the Clariostar Monochromator Microplate Reader (BMG Lab Technologies, Durham, NC). The release of LDH was calculated as a percentage of the untreated control.

Fluorescence histochemical analysis of cultured cortical neurons

For fluorescence histochemistry of cultured primary neurons, isolated cells were seeded onto poly-lysine treated 12 mm glass coverslips (placed in 12 well plates) and allowed to mature for 7 days in culture before glutamate treatment. Following treatment, cells were fixed in 4% paraformaldehyde for 20 min, permeabilized (10% goat serum in PBS containing 0.01% Triton-X) for 20 min and then blocked (10% goat serum in PBS) for 60 min. Cells were incubated with anti-CRMP2 antibody (diluted 1:1000 in block buffer) overnight at 4°C, then PBS washed, and incubated in an anti-rabbit-Alexa488 secondary antibody (1:500 in block buffer), anti-phalloidin-Tritc (1 µM, Sigma) and DAPI (1 µM, Sigma) for 60 min and a final PBS wash before being

mounted onto glass slides using antifade mounting media (Prolong Gold, Invitrogen). A Zeiss axioscope2 microscope using a 40X objective lens equipped with Zeiss HRc camera with filter sets for FITC (green) and Rhodamine (red) were used to take images for histological analysis. Identical settings and exposure time were used to capture images for both peptides. Images were processed using Zen blue software (Zeiss, Germany) to generate tiff images before importing them into ImageJ software (NIH, version 1.5b) and the number of blebs were counted in fields.

Cleavage of recombinant CaMKII by calpain-1 in vitro

For *in vitro* cleavage experiments of CaMKII, recombinant CaMKII was autophosphorylated prior to cleavage. Experiments were performed in digestion buffer (50 mM Tris-HCl, pH 7.4, 2 mM DTT, 30 mM NaCl, 10 mM $CaCl_2$). To generate pT286- CaMKIIα and pT287- GST-CaMKIIβ, 200 ng of the respective purified protein was stimulated with 10 μM ATP, 10 mM Mg^{2+}, 1.5 Ca^{2+} and 5 μM CaM at 30°C for 2 min. CaMKII proteins with and without prior autophosphorylation were incubated with calpain-1 (1 unit) for 45 min at 30 °C in digestion buffer, and digested sample were immediately analyzed by Western blot analysis as descried above.

Construction of spectral libraries of cultured cortical neurons and mouse brain tissues

For a data-dependent acquisition (DIA) based mass spectrometry experiment, it is essential we generate a library of identifiable peptides first using a standard data-dependent acquisition (DDA) approach (Figure S14). For the DIA type experiment to work, the identified peptides have to be in that library first. Excitotoxicity is a major mechanism of neuronal loss caused by ischemic stroke and traumatic brain injury. We therefore included the brains of sham-operated mice, brains of mice suffering DCAL ischemic stroke and traumatic brain injury to construct the spectral libraries and that is why the library contains pooled samples from the representative samples. Pre-fractionation of the pooled peptides was also performed to increase the number of identifiable peptides and generate a deeper library. Once we generated that library, all samples are analysed individually as a separate DIA experiment. The DIA approach then makes use of the generated library for identification and quantitation. This methodology allows for deeper identification and lower number of missing values.

Prior to quantitative analysis on the mass spectrometer, we built a spectral library, which contains all distinctive information of each identified peptides such as its retention time, charge

state and the fragment ion information. The success of the quantitation largely depends on the peptides to be quantified being present in this spectral library (Ludwig et al., 2018). As such, we pooled lysates from neurons with and without glutamate (100 µM) treatment for 30 min and 240 min together with brain lysates of mouse stroke and traumatic brain injury models. Briefly, proteins in the lysates were precipitated with cold acetone (-20°C) and then resuspended in 8 M urea in 50 mM triethylammonium bicarbonate (TEAB). Proteins are then reduced with 10 mM tris(2-carboxyethyl) phosphine Hydrochloride (TCEP), alkylated with 55 mM iodoacetamide, and digested with trypsin (trypsin to protein ratio of 1:50 (w/w)) overnight at 37°C. The resultant tryptic peptides were purified by solid phase extraction (SPE) (Oasis HBL cartridge, Waters). For global proteome analysis, 100µg of these peptides were fractionated into 8 fractions using the high pH reversed-phase fractionation kit (Pierce) according to the manufacturer's protocol before analysis on the Q-Exactive Orbitrap.

The LC system coupled to the Q-Eaxctive Orbitrap mass spectrometer was equipped with an Acclaim Pepmap nano-trap column (Dinoex-C18, 100 Å, 75 µm x 2 cm) and an Acclaim Pepmap RSLC analytical column (Dinoex-C18, 100 Å, 75 µm × 50 cm). After pre-fractionation with the high pH reversed-phase fractionation kit, tryptic peptides in each of the 8 fractions were injected to the enrichment column at an isocratic flow of 5 µl/min of 2 % (v/v) CH_3CN containing 0.1 % (v/v) formic acid for 6 min before the enrichment column was switched in-line with the analytical column. The eluents were 0.1 % (v/v) formic acid (Solvent A) and 100 % (v/v) CH_3CN in 0.1 % (v/v) formic acid (Solvent B). The flow gradient was (i) 0 - 6 min at 3 % Solvent B, (ii) 6 - 95 min, 3 – 20 % Solvent B (iii) 95 - 105 min, 20 – 40 % Solvent B (iv) 105 - 110 min, 40 – 80 % Solvent B (v) 110 - 115 min, 80 – 80 % Solvent B (vi) 115 - 117 min 85 – 3 % Solvent B and equilibrated at 3% Solvent B for 10 minutes before the next sample injection. In the Data-Dependent Acquisition (DDA) mode, full MS1 spectra were acquired in positive mode, 70 000 resolution from 300 - 1650 *m/z*, AGC target of $3e^6$ and maximum IT time of 50 ms. Fifteen of the most intense peptide ions with charge states ≥ 2 and intensity threshold of $1.7e^4$ were isolated for MSMS. The isolation window was set at 1.2 m/z and precursors fragmented using normalized collision energy of 30, 17 500 resolution, AGC target of $1e^5$ and maximum IT time of 100 ms. Dynamic exclusion was set to be 30 sec. In the Data Independent Acquisition (DIA) mode, the separation gradient was identical to that for DDA analysis. The QExactive plus mass spectrometer was operated in the hyper reaction monitoring/data independent (HRM/DIA) mode, whereby full

MS1 spectra were acquired in positive mode from 400 – 1000 *m/z*, 70 000 resolution, AGC target of $3e^6$ and maximum IT time of 50 ms. The isolation window was set at 21 *m/z* with a loop count of 30 and all precursors fragmented using normalized collision energy of 30, 17 500 resolution, AGC target of $1e^6$.

Analysis of global proteome of neurons

Neuronal lysates (500 µg) were mixed with cold acetone (-20°C) (1:5, v/v) in microfuge tubes and incubated at -20°C overnight to precipitate proteins. Acetone precipitated proteins (in control and treated lysates) were resuspended in 8 M urea in 50 mM TEAB (pH 8.0), and protein estimation was carried out using BCA assay (Pierce-Thermo Scientific) according to manufacturer's instruction. Equal amounts of protein were reduced with 10 mM tris-(2-carboxyethyl)-phosphine (TCEP) for 45 min at 37°C in a bench top vortex shaker. Reduced samples were alkylated with 55 mM iodoacetamide shaking 45 min at 37°C. Samples were diluted to 1 M urea (diluted with 25 mM TEAB) and digested with sequencing grade modified trypsin (1:50) overnight at 37°C. Digested samples were acidified to 1% (v/v) with pure formic acid, and solid phase extraction (SPE) was carried out with 60 mg Oasis HBL cartridge (Waters) to clean up the digested peptides. Briefly, the cartridge was washed with 80% acetonitrile (ACN) containing 0.1% trifluoroacetic acid (TFA) first and then with only 0.1% TFA before sample loading. Samples were washed again with 0.1% TFA and eluted with 800 µl 80% ACN containing 0.1% TFA. An aliquot (20 µg) of eluted peptides were freeze-dried overnight prior to analysis of changes in global proteome. For quantitative global proteomic analysis, 1 µg peptide in the presence of spiked-in iRT peptide was injected into the mass spectrometer and analysed using the HRM/DIA mode followed by analysis with the Spectronaut DIA-MS methodology and making use of the global proteome-specific spectral library built with the SEQUEST search engine incorporated in Proteome Discover (PD) (T. Wang et al., 2020) (Figure S14).

Analysis of the changes in neuronal N-terminome during excitotoxicity by the Terminal Amine Isotopic labelling of Substrates (TAILS) method

Neurons were treated with the neurotoxic concentration of glutamate (100 µM) for 30 min and 240 min. This toxic treatment strategy has been known to induce enhanced limited proteolysis

(referred to as proteolytic processing) as well as degradation of specific neuronal proteins by specific proteases activated in response to glutamate over-stimulation (referred to as excitotoxicity-activated proteases) (El-Gebali et al., 2019; Hossain et al., 2013). Proteins in the cell lysates of control (untreated) neurons and glutamate-treated neurons were precipitated by ice-cold acetone. After resuspension and denaturation in 8 M guanidinium hydrochloride in 100 mM HEPES, the neuronal proteins were reduced and alkylated. This is followed by isotopic dimethyl labelling of the free amino groups including the N^{α}-amino groups and ε-amino groups of the lysine side chains in the neuronal proteins. Proteins of the control neurons were labelled with formaldehyde (CH_2O) (referred to as light dimethyl labelled), while those of the glutamate-treated neurons were labelled with deuterated formaldehyde (CD_2O) (referred to as medium dimethyl labelled). Thus, the neo-N-termini of truncated protein fragments generated by proteolysis catalyzed by the excitotoxicity-activated proteases were medium dimethyl labelled (i.e., covalently linked with deuterated dimethyl groups). The light dimethyl labelled proteins from control neurons and the medium dimethyl labelled proteins from treated neurons were mixed at a ratio of 1:1 (w/w). The protein mixture was subjected to tryptic digestion. Tryptic peptides derived from the N-terminal end of neuronal proteins were devoid of free amino groups because the amino groups were either naturally blocked by modifications such as acetylation and myristoylation *in vivo* or by dimethylation *in vitro*. The other tryptic peptides derived from other parts of neuronal proteins contained the newly formed free N^{α}-amino group resulting from trypsinization. These peptides were selectively captured by the Hydroxy Polyglycerol Aldehyde (HPG-ALD) Polymer by reaction of their N^{α}-amino groups with the aldehyde (-CHO) groups of the polymer. After ultrafiltration to remove the complex of tryptic peptide-bound HPG-ALD polymers from the naturally modified and dimethyl labelled N-terminal peptides. The modified N-terminal peptides from each sample were pre-fractionated into 4 fractions SDB-RPS (styrene-divinylbenzene reverse phase sulfonate) based fractionation prior to LC-MS/MS analysis on the Orbitrap Elite mass spectrometer.

LC-MS/MS was carried out on LTQ Orbitrap Elite (Thermo Scientific) with a nanoESI interface in conjunction with an Ultimate 3000 RSLC nano HPLC (Dionex Ultimate 3000). The LC system was equipped with an Acclaim Pepmap nano-trap column (Dionex-C18, 100 Å, 75 µm x 2 cm) and an Acclaim Pepmap RSLC analytical column (Dionex-C18, 100 Å, 75 µm x 50 cm). The tryptic peptides were injected to the enrichment column at an isocratic flow of 5 µL/min of

3% v/v CH_3CN containing 0.1% v/v formic acid for 5 min before the enrichment column was switched in-line with the analytical column. The eluents were 0.1% v/v formic acid (solvent A) and 100% v/v CH_3CN in 0.1% v/v formic acid (solvent B). The flow gradient was (i) 0-6 min at 3% B, (ii) 6-95 min, 3-20% B (iii) 95-105 min, 20- 40% B (iv) 105-110 min, 40-80% B (v) 110-115 min, 80-80% B (vi) 115-117 min 85-3% and equilibrated at 3% B for 10 minutes before the next sample injection. The LTQ Orbitrap Elite spectrometer was operated in the data-dependent mode with nanoESI spray voltage of 1.8kV, capillary temperature of 250°C and S-lens RF value of 55%. All spectra were acquired in positive mode with full scan MS spectra from *m/z* 300-1650 in the FT mode at 240,000 resolution. Automated gain control was set to a target value of 1.0e6. Lock mass of 445.120025 was used. The top 20 most intense precursors were subjected to rapid collision induced dissociation (rCID) with the normalized collision energy of 30 and activation q of 0.25. Dynamic exclusion with of 30 seconds was applied for repeated precursors.

Synthesis of FITC-Tat-Src peptide

Peptides were constructed on a CEM Liberty 12-Channel Automated Microwave Peptide Synthesizer using Fmoc-PAL-PEG-PS^{TM} (Rink resin; loading capacity 0.21 mmol/g) (ThermoFisher, Cat.#: GEN913383) and Fmoc-protected amino acids (GL Biochem (Shanghai)). Fmoc deprotections were performed using 20% piperidine in DMF. Activation of Fmoc-amino acids was achieved using a 0.5 M solution of HCTU (2-(6-chloro-1H-benzotriazole-1-yl)-1,1,3,3-tetramethylaminium hexafluorophosphate) and DIPEA (diisopropylethylamine) in DMF in a ratio of 2 ml:2 ml:0.34 ml per 1 mmol of Fmoc amino acid used. Peptide coupling and deprotection efficiency was monitored using a 2,4,6-trinitrobenzene-sulfonic acid (TNBSA) assay (Hancock & Battersby, 1976). The FITC-Tat-ahx-Src 49-79 peptide (FITC-Tat-Src) was synthesized sequentially as two main parts with aminohexanoic acid linker used between the two main sequences. First, the sequence ahx-Src 49-79 was synthesized. The synthesized peptide was validated via ESI-MS and RP-HPLC. Then, the Tat peptide with sequence ahx-GRKKRRQRRRPQ was continued on the ahx-Src 49-79 sequence while still on resin to generate ahx-Tat-ahx-Src 49-79 peptide-resin. Fluorescein isothiocyanate (FITC) was coupled to ahx-Tat-ahx-Src 49-79 peptide-resin using HCTU and DIPEA. The peptide was cleaved from the resin using TFA/triisopropylsilane/H_2O mixture (volume ratio of 95:2.5:2.5) for 90 min. Excess TFA was removed via evaporation with stream of N_2 gas. The peptide was precipitated by addition of

diethyl ether. The mixture was then centrifuged and the ether decanted. The pellet containing the peptide was re-dissolved in 30% acetonitrile/H_2O and filtered through a 0.22 μm filter. The crude peptide solution was lyophilized prior to purification by semi-preparative RP-HPLC. Fractions containing the pure peptide were pooled and lyophilized. The dried peptide was stored at 4 °C until further use. The purified peptide was analyzed and validated via ESI-MS with mass [M + H^+] of 5385.4 Da and RP-HPLC shown as a single peak in HPLC chromatogram.

Quantification and statistical analysis of proteomics data

Quantitation of global proteomic changes in mouse primary cortical neurons induced by glutamate treatment

Protein/peptide identification from the DDA-based analysis and subsequent spectral library generation were conducted using Proteome Discoverer (v.2.1, Thermo Fischer Scientific) with the Sequest HT search engine in combination with the Percolator semi-supervised learning algorithm (Kall, Canterbury, Weston, Noble, & MacCoss, 2007) and PhosphoRS (Taus et al., 2011) or with MaxQuant software utilizing the Andromeda search engine (Tyanova et al., 2016) on M*us musculus* protein database (SwissProt (TaxID = 10090)(version 2017-10-25)) (Figure S14). The search parameters were: a precursor tolerance of 20 ppm, MSMS tolerance of 0.05 Da, fixed modifications of carbamidomethylation of cysteine (+57 Da), methionine oxidation (+16 Da) or phosphorylation of serine, threonine and tyrosine (+80Da) . Peptides were accepted based on a FDR of <0.01 at both the peptide and protein levels.

DIA based quantitative analysis was carried out using the Spectronaut software (Spectronaut 11, Biognosys). To build the spectral library in Spectronaut based on MaxQuant and Proteome Discoverer results, all the default parameters were used except that best N-terminal fragments per peptide was set to minimum 5 and maximum 20. Two spectral libraries were built for phosphopeptides whereas one library from the search results of Proteome Discoverer was built for the global library. The spectral libraries for peptides are generated identically (Figure S14). The DIA files for each sample were converted to htrms format sing HTRMS Converter (Biognosy) and loaded on Spectronaut 11 for generation of protein intensities. The default parameters were used for data extraction, XIC extraction, calibration, identification, and protein inference. The iRT profiling strategy was used with unify peptide peak options enabled. For quantitation of the trptic

peptides unique to each protein, the Q value percentile of 0.75 was set. Quantitation is based on stripped sequence, and global normalization was performed. The Spectronaut results output were further processed with Perseus software (version 1.6) (Tyanova & Cox, 2018).

Classification of the N-terminal peptides identified and quantified by TAILS method

Using the TAILS method (Kleifeld et al., 2011), we identified and quantified (i) the "natural" free N-termini of mature proteins biosynthesized in physiological conditions, and (ii) the newly formed neo-N-termini of stable truncated protein fragments and intermediate peptide fragments generated by proteolysis of neuronal proteins during excitotoxicity. Of the quantifiable N-terminal peptides identified by the TAILS analysis of excitotoxic neurons, over 2,300 contained acetylated N-termini and over 2,600 contained dimethyl labelled N-termini (Figures 1A and S6, Tables S6A and S7A). Whereas the acetylated N-terminal peptides were derived from intact proteins undergoing N-terminal acetylation during biosynthesis and maturation in neurons, the dimethyl-labelled N-terminal peptides were derived from free N-termini of neuronal proteins *in vitro* via the TAILS procedure. The dimethyl labelled N-terminal peptides were further sub-divided into four groups: (i) those retaining the first methionine encoded by the start codon (+ Met); (ii) those with the start codon-encoded methionine removed (-Met); (iii) those with the N-terminal signal peptide segments removed during maturation of the parental neuronal proteins *in vivo* (-signal peptide); and (iv) those containing neo-N-termini generated by proteolysis of intact mature neuronal proteins (Neo) (Figure 1A). We focused our further analysis on the neo-N-terminal peptides as they revealed both the cleavage sites and identities of neuronal proteins undergoing proteolysis during excitotoxicity. Based on the rationale depicted in Figure 1C, neo-N-terminal peptides exhibiting increased abundance were assigned as those derived from the stable truncated protein fragments generated from enhanced proteolytic processing of neuronal proteins during excitotoxicity. Neo-N-terminal peptides exhibiting decreased abundance were assigned as being derived from neuronal proteins undergoing enhanced degradation for clearance during excitotoxicity.

Determination of the abundance ratio cut-off values to identify neuronal proteins exhibiting significantly enhanced proteolysis induced by treatment with glutamate or co-treatment with glutamate and calpeptin

Over 2,000 neo-N-terminal peptides were found by the TAILS method to be generated by enhanced proteolysis during excitotoxicity (Figure 1A). Figures S2 and S6 depict results of our statistical analysis to calculate the thresholds for their assignment to be neo-N-terminal peptides generated by significantly enhanced degradation and those generated by significantly enhanced proteolytic processing of neuronal proteins during excitotoxicity. Based upon the normalized distribution of the $\log_2$ M/L ratios of the identified neo-N-terminal peptides, we determined the median and standard deviations (S.D.) of the distribution of the $\log_2$ M/L ratios. Statistically, values that are outside the 1.5 interquartile range (IQR) are considered as outliers (Tukey, 1977) (Figure S2A). The 1.5×IQR values can be calculated as 5 × S.D. of the distributions of the abundance ratios ($\log_2$ M/L ratios) of all quantifiable N-terminal peptides (Figure S2B). Using the Tukey's 1.5 × interquartile range (IQR) rule (Tukey, 1977), we determined the abundance ratio cut-off values (M/L) for the neo-N-terminal peptides exhibiting significantly reduced abundance and those exhibiting significantly increased abundance during excitotoxicity (Figure S2A).

To determine the abundance ratio cut-off values to identify the neo-N-terminal peptides generated by significant proteolysis by neuronal proteases activated in response to co-treatment with glutamate and calpeptin, the M/L ratio cut-off values equivalent to 1.5 interquartile range (IQR) were calculated. As depicted in Figure S6A, for the N-terminal peptides co-treated for 30 min, the lower and upper cut-off values were 0.271 and 3.8 (i.e. M/L ≥ 3.8 for the neo-N-terminal peptides generated by significantly enhanced proteolytic processing and M/L ≤ 0.271 for those generated by significantly enhanced degradation). For those derived from neurons co-treated for 240 min, the lower and upper cut-off values were 0.386 and 2.876, respectively.

Key resources

The antibodies used in our studies include: rabbit polyclonal anti-CRMP2 antibody (RRID: AB_2094339; Cat. No.: 9393; Cell Signaling Technology), rabbit polyclonal anti-CRMP2 (phospho T509) antibody (Cat. No.: ab192799; Abcam), anti-DCLK1 (anti-DCMKL1) antibody against amino acids 679-729 near the C-terminus of DCLK1 (Cat. No.: ab106635; Abcam), mouse

anti-Src Mab327 antibody (RRID: AB_443522; Cat. No.: ab16885; Abcam), anti-CD11b (Clone OX-42) mouse monoclonal antibody (Cat. No.: MCA275G; BioRad (formerly serotec)), NeuN rabbit polyclonal antibody (RRID: AB_10807945; Cat. No.: ABN78; MERK Millipore (Sigma Aldrich)), anti-GFAP mouse monoclonal antibody (Clone GA5) (RRID: AB_11212597; Cat. No.: MAB360; MERK Millipore (Sigma Aldrich), CaMKIIα (#NB100-1983, RRID:AB_10001339; mouse monoclonal IgG, clone 6g9, Novus Biologicals), CaMKII (pan) (#4436, RRID:AB_1054545; rabbit monoclonal IgG, clone D11A10, Cell Signaling Technology), beta-Actin (#ab6276, RRID: AB_2223210; mouse monoclonal IgG, cloneAC-15, Abcam), CaMKIIβ (#ab34703, RRID:AB_2275072; rabbit polyclonal antibody, Abcam); Goat anti-mouse Alexa Fluor Plus 800 (#A32730, RRID: AB_2633279; polyclonal IgG, Invitrogen) and donkey anti-rabbit Alexa Fluor Plus 488 (#A32790, RRID: AB_2762833; polyclonal IgG, Invitrogen).

The following recombinant proteins were used: CaMKIIα (#PR4586C, Invitrogen), GST-CaMKIIβ (#02-110, Carna biosciences) and Calpain-1 (#208713-500UG, Calbiochem).

Chemicals and reagents specifically used for proteomic analysis include: Pierce™ high pH reversed-phase peptide fractionation kit (Cat. No.: 84868; ThermoFisher), High-Select™ Fe-NTA phosphopeptide enrichment kit (Cat. No.: A32992; ThermoFisher), titansphere phos-TiO_2 (Cat. No.: 5010-21315; GL Sciences), triehylammonium bicarbonate (TEAB) buffer (Cat. No.:5010-21315; Sigma), formaldehyde (DLM-805-PK (CD_2O) ULM-9498-PK (CH_2O), Cambridge Isotope) and hydroxy polyglycerol aldehyde (HPG-ALD) polymer (UBC.FLINTBOX https://ubc.flintbox.com/#technologies/888fc51c-36c0-40dc-a5c9-0f176ba68293).

The chemicals used for synthesis of the cell permeable TAT-Src, TAT-Scrambled and fluorescent TAT-Src peptides include: Fmoc-PAL-PEG-PS™ (Rink resin; loading capacity 0.21 mmol/g) (Cat. No.: GEN913383; ThermoFisher), Fmoc-protected amino acids (GL Biochem (Shanghai)), phalloidin–tetramethylrhodamine B isothiocyanate (Phalloidin-Tritc) (Cat. No.: Sigma P1951; Merck).

The animals used in our studies including (i) C57BL/6 mice (pregnant and at gestational day 14-15) used for cultured primary cortical neurons (ii) C57BL/6 mice used for construction of spectral libraries and (iii) Male hooded Wistar rats for the in vivo model of neurotoxicity were sourced from Animal Resources Centre, Canning Vale WA 6970 Australia (iv) male C57BL/6*J* were obtained from the Biomedical Research Facility, University of Otago, New

Zealand and *Camk2a*$^{-/-}$ mice (*Camk2*^{atm3Sva}, MGI:2389262) mice backcrossed into the C57BL/6*J* background were bread in the In Vivo Pharmacology Research Unit, University of Copenhagen, Denmark for the use in photothrombotic stroke surgeries.

The software and algorithms used in our studies are: Proteome Discoverer (Thermo Scientific; RRID: SCR_014477), MaxQuant (RRID: SCR_014485), Spectronaut (Spectronaut 11) (Biognosys), PhosphoSitePlus: Protein Modification Site (Cell Signaling Technology; RRID: SCR_001837), Image J (RRID: SCR_003070), QIAGEN Ingenuity Pathway Analysis (Qiagen) and SynGO (RRID:SCR_017330), the protein interaction resource derived from cross-linking mass spectrometry database of synaptosome and microsome fractions purified from hippocampus and cerebellum of mouse brains (Gonzalez-Lozano et al., 2020) and String database (Szklarczyk et al., 2019)

Acknowledgments

We thank Robert Qi, Swati Varshney and Anderly Chueh for comments and suggestions for drafting this manuscript.

Funding: This work was funded by grants from the National Health and Medical Research Council (NHMRC) of Australia, NSERC of Canada, Australian Brain Foundation and Israel Science Foundation: NHMRC project grant #1050486 to H.-C.C.; NHMRC project grant #1141906 to A. Dhillon; NSERC discovery grant #DGECR-2019-0012); grants from the Israel Science Foundation (1623/17 and 2167/17) to O.K. and Australian Brain Foundation grant to P.P. and H.-C.C. The Lundbeck Foundation (R277-2018-260) to P.W., A.N.C. and N. G.-K. and the Novo Nordisk Foundation (NNF14CC0001) to P.W. and N. G.-K.

Author Contributions: S.S.A. and C.-S.A. conceptualized, designed, performed, and analyzed most of the experiments and co-wrote the paper. H.-C.C., N.A.W., A.D., O.K., G.D.C. and C.R. conceptualized, designed and analyzed the proteomic data, neuronal cell biology data or data of in vivo model of neurotoxicity. M.I.H., M.A.K., H.-J.Z., G.D.C., A.H., L.B. and C.R. conceptualized, designed and performed the experiments of excitotoxic cell death of cultured neurons and effects of Tat-Src and Tat-Scrambled peptides on neuronal loss in vivo. N.G.-K. A.N.C and P.W. contributed to generation and interpretation of *in vitro* and *in vivo* data of CaMKII. S.S.A., H.-C.C., C.-S.A., N.A.W., S.S., H.N., R.M. and D.D. performed experiments to generate the spectral libraries for DIA proteomic analysis of the changes in global and phospho-proteomes of neurons. M.L., H.-C.C., A.D., O.K. N.A.W. and C.-S.A. analyzed the N-terminomic data to define the potential substrates of calpains in neurons. H.-C.C. and P.P. performed the SynGO analysis to assign the synaptic locations and biological processes of the

significantly modified proteins. D.L., H.-J.Z., A. Dhillon, A. Dufour, I.S.L. P.P. F.B. A.N.C. and J.P.L. conceptualized, interpreted experimental data on excitotoxic neuronal death and experimental validation of the proteomic results and co-wrote the paper.

Competing interest*:* The authors declare no competing interest.

Data and materials availability*:* The mass spectrometry proteomics data have been deposited to the ProteomeXchange Consortium via the PRIDE (Perez-Riverol et al., 2019) partner repository with the dataset identifiers PXD019211 for the project entitled "N-terminomics Analysis of Mouse cultured cortical neuron treated with glutamate", and PXD019527 for the project entitled "Phosphoproteomics of mouse cortical neuron".

Aarts, M., Liu, Y., Liu, L., Besshoh, S., Arundine, M., Gurd, J. W., . . . Tymianski, M. (2002). Treatment of ischemic brain damage by perturbing NMDA receptor- PSD-95 protein interactions. *Science, 298*(5594), 846-850. doi:10.1126/science.1072873

Ali, D. W., & Salter, M. W. (2001). NMDA receptor regulation by Src kinase signalling in excitatory synaptic transmission and plasticity. *Curr Opin Neurobiol, 11*(3), 336-342. doi:S0959-4388(00)00216-6 [pii]

Ballarin, B., & Tymianski, M. (2018). Discovery and development of NA-1 for the treatment of acute ischemic stroke. *Acta Pharmacol Sin, 39*(5), 661-668. doi:10.1038/aps.2018.5

Baudry, M., & Bi, X. (2016). Calpain-1 and Calpain-2: The Yin and Yang of Synaptic Plasticity and Neurodegeneration. *Trends Neurosci, 39*(4), 235-245. doi:10.1016/j.tins.2016.01.007

Bayer, K. U., Lohler, J., Schulman, H., & Harbers, K. (1999). Developmental expression of the CaM kinase II isoforms: ubiquitous gamma- and delta-CaM kinase II are the early isoforms and most abundant in the developing nervous system. *Brain Res Mol Brain Res, 70*(1), 147-154. doi:10.1016/s0169-328x(99)00131-x

Bayer, K. U., & Schulman, H. (2019). CaM Kinase: Still Inspiring at 40. *Neuron, 103*(3), 380-394. doi:10.1016/j.neuron.2019.05.033

Bhattacharyya, M., Karandur, D., & Kuriyan, J. (2020). Structural Insights into the Regulation of Ca(2+)/Calmodulin-Dependent Protein Kinase II (CaMKII). *Cold Spring Harb Perspect Biol, 12*(6). doi:10.1101/cshperspect.a035147

Bian, Y., Li, L., Dong, M., Liu, X., Kaneko, T., Cheng, K., . . . Zou, H. (2016). Ultra-deep tyrosine phosphoproteomics enabled by a phosphotyrosine superbinder. *Nat Chem Biol, 12*(11), 959-966. doi:10.1038/nchembio.2178

Brennan, A. M., Suh, S. W., Won, S. J., Narasimhan, P., Kauppinen, T. M., Lee, H., . . . Swanson, R. A. (2009). NADPH oxidase is the primary source of superoxide induced by NMDA receptor activation. *Nat Neurosci, 12*(7), 857-863. doi:nn.2334 [pii]
10.1038/nn.2334

Buonarati, O. R., Cook, S. G., Goodell, D. J., Chalmers, N. E., Rumian, N. L., Tullis, J. E., . . . Bayer, K. U. (2020). CaMKII versus DAPK1 Binding to GluN2B in Ischemic Neuronal Cell Death after Resuscitation from Cardiac Arrest. *Cell Rep, 30*(1), 1-8 e4. doi:10.1016/j.celrep.2019.11.076

Buonarati, O. R., Miller, A. P., Coultrap, S. J., Bayer, K. U., & Reichow, S. L. (2021). Conserved and divergent features of neuronal CaMKII holoenzyme structure, function, and high-order assembly. *Cell Rep, 37*(13), 110168. doi:10.1016/j.celrep.2021.110168

Burgess, H. A., & Reiner, O. (2001). Cleavage of doublecortin-like kinase by calpain releases an active kinase fragment from a microtubule anchorage domain. *J Biol Chem, 276*(39), 36397-36403. doi:10.1074/jbc.M105153200

Chamorro, A., Lo, E. H., Renu, A., van Leyen, K., & Lyden, P. D. (2021). The future of neuroprotection in stroke. *J Neurol Neurosurg Psychiatry, 92*(2), 129-135. doi:10.1136/jnnp-2020-324283

Chen, Y., Brennan-Minnella, A. M., Sheth, S., El-Benna, J., & Swanson, R. A. (2015). Tat-NR2B9c prevents excitotoxic neuronal superoxide production. *J Cereb Blood Flow Metab, 35*(5), 739-742. doi:10.1038/jcbfm.2015.16

Choi, D. W. (1988). Glutamate neurotoxicity and diseases of the nervous system. *Neuron, 1*(8), 623-634. doi:0896-6273(88)90162-6 [pii]

Choi, D. W. (1990). Methods for antagonizing glutamate neurotoxicity. *Cerebrovasc Brain Metab Rev, 2*(2), 105-147.

Choi, D. W. (2020). Excitotoxicity: Still Hammering the Ischemic Brain in 2020. *Front Neurosci, 14*, 579953. doi:10.3389/fnins.2020.579953

Chow, H. M., Guo, D., Zhou, J. C., Zhang, G. Y., Li, H. F., Herrup, K., & Zhang, J. (2014). CDK5 activator protein p25 preferentially binds and activates GSK3beta. *Proc Natl Acad Sci U S A, 111*(45), E4887-4895. doi:10.1073/pnas.1402627111

Clarkson, A. N., Huang, B. S., Macisaac, S. E., Mody, I., & Carmichael, S. T. (2010). Reducing excessive GABA-mediated tonic inhibition promotes functional recovery after stroke. *Nature, 468*(7321), 305-309. doi:10.1038/nature09511

Cook, D. J., Teves, L., & Tymianski, M. (2012). A translational paradigm for the preclinical evaluation of the stroke neuroprotectant Tat-NR2B9c in gyrencephalic nonhuman primates. *Sci Transl Med, 4*(154), 154ra133. doi:10.1126/scitranslmed.3003824

Cuerrier, D., Moldoveanu, T., & Davies, P. L. (2005). Determination of peptide substrate specificity for mu-calpain by a peptide library-based approach: the importance of primed side interactions. *J Biol Chem, 280*(49), 40632-40641. doi:10.1074/jbc.M506870200

Deng, G., Orfila, J. E., Dietz, R. M., Moreno-Garcia, M., Rodgers, K. M., Coultrap, S. J., . . . Herson, P. S. (2017). Autonomous CaMKII Activity as a Drug Target for Histological and Functional Neuroprotection after Resuscitation from Cardiac Arrest. *Cell Rep, 18*(5), 1109-1117. doi:10.1016/j.celrep.2017.01.011

duVerle, D. A., & Mamitsuka, H. (2019). CalCleaveMKL: a Tool for Calpain Cleavage Prediction. *Methods Mol Biol, 1915*, 121-147. doi:10.1007/978-1-4939-8988-1_11

El-Gebali, S., Mistry, J., Bateman, A., Eddy, S. R., Luciani, A., Potter, S. C., . . . Finn, R. D. (2019). The Pfam protein families database in 2019. *Nucleic Acids Res, 47*(D1), D427-D432. doi:10.1093/nar/gky995

Endo, H., Nito, C., Kamada, H., Nishi, T., & Chan, P. H. (2006). Activation of the Akt/GSK3beta signaling pathway mediates survival of vulnerable hippocampal neurons after transient global cerebral ischemia in rats. *J Cereb Blood Flow Metab, 26*(12), 1479-1489. doi:10.1038/sj.jcbfm.9600303

Evsyukova, I., Plestant, C., & Anton, E. S. (2013). Integrative mechanisms of oriented neuronal migration in the developing brain. *Annu Rev Cell Dev Biol, 29*, 299-353. doi:10.1146/annurev-cellbio-101512-122400

Fisher, M., & Savitz, S. I. (2022). Pharmacological brain cytoprotection in acute ischaemic stroke - renewed hope in the reperfusion era. *Nat Rev Neurol*. doi:10.1038/s41582-021-00605-6

Fricker, M., Tolkovsky, A. M., Borutaite, V., Coleman, M., & Brown, G. C. (2018). Neuronal Cell Death. *Physiol Rev, 98*(2), 813-880. doi:10.1152/physrev.00011.2017

Fujikawa, D. G. (2015). The role of excitotoxic programmed necrosis in acute brain injury. *Comput Struct Biotechnol J, 13*, 212-221. doi:10.1016/j.csbj.2015.03.004

Ginet, V., Spiehlmann, A., Rummel, C., Rudinskiy, N., Grishchuk, Y., Luthi-Carter, R., . . . Puyal, J. (2014). Involvement of autophagy in hypoxic-excitotoxic neuronal death. *Autophagy, 10*(5), 846-860. doi:10.4161/auto.28264

Gleeson, J. G., Lin, P. T., Flanagan, L. A., & Walsh, C. A. (1999). Doublecortin is a microtubule-associated protein and is expressed widely by migrating neurons. *Neuron, 23*(2), 257-271. doi:10.1016/s0896-6273(00)80778-3

Gonzalez-Lozano, M. A., Koopmans, F., Sullivan, P. F., Protze, J., Krause, G., Verhage, M., . . . Smit, A. B. (2020). Stitching the synapse: Cross-linking mass spectrometry into resolving synaptic protein interactions. *Sci Adv, 6*(8), eaax5783. doi:10.1126/sciadv.aax5783

Greenwood, S. M., Mizielinska, S. M., Frenguelli, B. G., Harvey, J., & Connolly, C. N. (2007). Mitochondrial dysfunction and dendritic beading during neuronal toxicity. *J Biol Chem, 282*(36), 26235-26244. doi:10.1074/jbc.M704488200

Guo, X., & Chen, B. (2022). Investigating the role of Ca(2+)/calmodulin-dependent protein kinase II in the survival of retinal ganglion cells. *Neural Regen Res, 17*(5), 1001-1002. doi:10.4103/1673-5374.324844

Hancock, W. S., & Battersby, J. E. (1976). A new micro-test for the detection of incomplete coupling reactions in solid-phase peptide synthesis using 2,4,6-trinitrobenzenesulphonic acid. *Anal Biochem, 71*(1), 260-264. doi:10.1016/0003-2697(76)90034-8

Hasbani, M. J., Schlief, M. L., Fisher, D. A., & Goldberg, M. P. (2001). Dendritic spines lost during glutamate receptor activation reemerge at original sites of synaptic contact. *J Neurosci, 21*(7), 2393-2403.

Hayashi, Y., Shi, S. H., Esteban, J. A., Piccini, A., Poncer, J. C., & Malinow, R. (2000). Driving AMPA receptors into synapses by LTP and CaMKII: requirement for GluR1 and PDZ domain interaction. *Science, 287*(5461), 2262-2267. doi:10.1126/science.287.5461.2262

Hill, M. D., Goyal, M., Menon, B. K., Nogueira, R. G., McTaggart, R. A., Demchuk, A. M., . . . Investigators, E.-N. (2020). Efficacy and safety of nerinetide for the treatment of acute ischaemic stroke (ESCAPE-NA1): a multicentre, double-blind, randomised controlled trial. *Lancet, 395*(10227), 878-887. doi:10.1016/S0140-6736(20)30258-0

Hill, M. D., Martin, R. H., Mikulis, D., Wong, J. H., Silver, F. L., Terbrugge, K. G., . . . investigators, E. t. (2012). Safety and efficacy of NA-1 in patients with iatrogenic stroke after endovascular aneurysm repair (ENACT): a phase 2, randomised, double-blind, placebo-controlled trial. *Lancet Neurol, 11*(11), 942-950. doi:10.1016/S1474-4422(12)70225-9

Hoque, A., Williamson, N. A., Ameen, S. S., Ciccotosto, G. D., Hossain, M. I., Oakhill, J. S., . . . Cheng, H. C. (2019). Quantitative proteomic analyses of dynamic signalling events in cortical neurons undergoing excitotoxic cell death. *Cell Death Dis, 10*(3), 213. doi:10.1038/s41419-019-1445-0

Hosie, K. A., King, A. E., Blizzard, C. A., Vickers, J. C., & Dickson, T. C. (2012). Chronic excitotoxin-induced axon degeneration in a compartmented neuronal culture model. *ASN Neuro, 4*(1). doi:10.1042/AN20110031

Hossain, M. I., Roulston, C. L., Kamaruddin, M. A., Chu, P. W., Ng, D. C., Dusting, G. J., . . . Cheng, H. C. (2013). A truncated fragment of Src protein kinase generated by calpain-mediated cleavage is a mediator of neuronal death in excitotoxicity. *J Biol Chem, 288*(14), 9696-9709. doi:10.1074/jbc.M112.419713

Inagaki, N., Chihara, K., Arimura, N., Menager, C., Kawano, Y., Matsuo, N., . . . Kaibuchi, K. (2001). CRMP-2 induces axons in cultured hippocampal neurons. *Nat Neurosci, 4*(8), 781-782. doi:10.1038/90476

Jiang, S. X., Kappler, J., Zurakowski, B., Desbois, A., Aylsworth, A., & Hou, S. T. (2007). Calpain cleavage of collapsin response mediator proteins in ischemic mouse brain. *Eur J Neurosci, 26*(4), 801-809. doi:10.1111/j.1460-9568.2007.05715.x

Kall, L., Canterbury, J. D., Weston, J., Noble, W. S., & MacCoss, M. J. (2007). Semi-supervised learning for peptide identification from shotgun proteomics datasets. *Nat Methods, 4*(11), 923-925. doi:10.1038/nmeth1113

Kleifeld, O., Doucet, A., auf dem Keller, U., Prudova, A., Schilling, O., Kainthan, R. K., . . . Overall, C. M. (2010). Isotopic labeling of terminal amines in complex samples identifies protein N-termini and protease cleavage products. *Nat Biotechnol, 28*(3), 281-288. doi:10.1038/nbt.1611

Kleifeld, O., Doucet, A., Prudova, A., auf dem Keller, U., Gioia, M., Kizhakkedathu, J. N., & Overall, C. M. (2011). Identifying and quantifying proteolytic events and the natural N terminome by terminal amine isotopic labeling of substrates. *Nat Protoc, 6*(10), 1578-1611. doi:10.1038/nprot.2011.382

Kondo, S., Takahashi, K., Kinoshita, Y., Nagai, J., Wakatsuki, S., Araki, T., . . . Ohshima, T. (2019). Genetic inhibition of CRMP2 phosphorylation at serine 522 promotes axonal regeneration after optic nerve injury. *Sci Rep, 9*(1), 7188. doi:10.1038/s41598-019-43658-w

Kool, M. J., Proietti Onori, M., Borgesius, N. Z., van de Bree, J. E., Elgersma-Hooisma, M., Nio, E., . . . van Woerden, G. M. (2019). CAMK2-Dependent Signaling in Neurons Is Essential for Survival. *J Neurosci, 39*(28), 5424-5439. doi:10.1523/JNEUROSCI.1341-18.2019

Koopmans, F., van Nierop, P., Andres-Alonso, M., Byrnes, A., Cijsouw, T., Coba, M. P., . . . Verhage, M. (2019). SynGO: An Evidence-Based, Expert-Curated Knowledge Base for the Synapse. *Neuron, 103*(2), 217-234 e214. doi:10.1016/j.neuron.2019.05.002

Kwiatkowski, A. P., & King, M. M. (1989). Autophosphorylation of the type II calmodulin-dependent protein kinase is essential for formation of a proteolytic fragment with catalytic activity. Implications for long-term synaptic potentiation. *Biochemistry, 28*(13), 5380-5385. doi:10.1021/bi00439a010

Lankiewicz, S., Marc Luetjens, C., Truc Bui, N., Krohn, A. J., Poppe, M., Cole, G. M., . . . Prehn, J. H. (2000). Activation of calpain I converts excitotoxic neuron death into a caspase-independent cell death. *J Biol Chem, 275*(22), 17064-17071.

Leurs, U., Klein, A. B., McSpadden, E. D., Griem-Krey, N., Solbak, S. M. O., Houlton, J., . . . Wellendorph, P. (2021). GHB analogs confer neuroprotection through specific interaction with the CaMKIIalpha hub domain. *Proc Natl Acad Sci U S A, 118*(31). doi:10.1073/pnas.2108079118

Lipton, S. A. (2007). Pathologically activated therapeutics for neuroprotection. *Nat Rev Neurosci, 8*(10), 803-808. doi:10.1038/nrn2229

Liu, D. Z., Waldau, B., Ander, B. P., Zhan, X., Stamova, B., Jickling, G. C., . . . Sharp, F. R. (2017). Inhibition of Src family kinases improves cognitive function after intraventricular hemorrhage or intraventricular thrombin. *J Cereb Blood Flow Metab, 37*(7), 2359-2367. doi:10.1177/0271678X16666291

Liu, Z., Cao, J., Gao, X., Ma, Q., Ren, J., & Xue, Y. (2011). GPS-CCD: a novel computational program for the prediction of calpain cleavage sites. *PLoS One, 6*(4), e19001. doi:10.1371/journal.pone.0019001

Liu, Z. X., Yu, K., Dong, J., Zhao, L., Liu, Z., Zhang, Q., . . . Cheng, H. (2019). Precise Prediction of Calpain Cleavage Sites and Their Aberrance Caused by Mutations in Cancer. *Front Genet, 10*, 715. doi:10.3389/fgene.2019.00715

Lu, F., Shao, G., Wang, Y., Guan, S., Burlingame, A. L., Liu, X., . . . Jiang, X. (2018). Hypoxia-ischemia modifies postsynaptic GluN2B-containing NMDA receptor complexes in the neonatal mouse brain. *Exp Neurol, 299*(Pt A), 65-74. doi:10.1016/j.expneurol.2017.10.005

Ludwig, C., Gillet, L., Rosenberger, G., Amon, S., Collins, B. C., & Aebersold, R. (2018). Data-independent acquisition-based SWATH-MS for quantitative proteomics: a tutorial. *Mol Syst Biol, 14*(8), e8126. doi:10.15252/msb.20178126

Meyer, D. A., Torres-Altoro, M. I., Tan, Z., Tozzi, A., Di Filippo, M., DiNapoli, V., . . . Bibb, J. A. (2014). Ischemic stroke injury is mediated by aberrant Cdk5. *J Neurosci, 34*(24), 8259-8267. doi:10.1523/JNEUROSCI.4368-13.2014

Miller, S. G., & Kennedy, M. B. (1986). Regulation of brain type II Ca2+/calmodulin-dependent protein kinase by autophosphorylation: a Ca2+-triggered molecular switch. *Cell, 44*(6), 861-870. doi:10.1016/0092-8674(86)90008-5

Moldoveanu, T., Campbell, R. L., Cuerrier, D., & Davies, P. L. (2004). Crystal structures of calpain-E64 and -leupeptin inhibitor complexes reveal mobile loops gating the active site. *J Mol Biol, 343*(5), 1313-1326. doi:10.1016/j.jmb.2004.09.016

Nawabi, H., Belin, S., Cartoni, R., Williams, P. R., Wang, C., Latremoliere, A., . . . He, Z. (2015). Doublecortin-Like Kinases Promote Neuronal Survival and Induce Growth Cone Reformation via Distinct Mechanisms. *Neuron, 88*(4), 704-719. doi:10.1016/j.neuron.2015.10.005

Niwa, S., Nakamura, F., Tomabechi, Y., Aoki, M., Shigematsu, H., Matsumoto, T., . . . Nitta, R. (2017). Structural basis for CRMP2-induced axonal microtubule formation. *Sci Rep, 7*(1), 10681. doi:10.1038/s41598-017-11031-4

Olney, J. W. (1969). Brain lesions, obesity, and other disturbances in mice treated with monosodium glutamate. *Science, 164*(3880), 719-721.

Ono, Y., Saido, T. C., & Sorimachi, H. (2016). Calpain research for drug discovery: challenges and potential. *Nat Rev Drug Discov, 15*(12), 854-876. doi:10.1038/nrd.2016.212

Osborne, K. A., Shigeno, T., Balarsky, A. M., Ford, I., McCulloch, J., Teasdale, G. M., & Graham, D. I. (1987). Quantitative assessment of early brain damage in a rat model of focal cerebral ischaemia. *J Neurol Neurosurg Psychiatry, 50*(4), 402-410. doi:10.1136/jnnp.50.4.402

Parsons, M. P., & Raymond, L. A. (2014). Extrasynaptic NMDA receptor involvement in central nervous system disorders. *Neuron, 82*(2), 279-293. doi:10.1016/j.neuron.2014.03.030

Patel, O., Dai, W., Mentzel, M., Griffin, M. D., Serindoux, J., Gay, Y., . . . Lucet, I. S. (2016). Biochemical and Structural Insights into Doublecortin-like Kinase Domain 1. *Structure, 24*(9), 1550-1561. doi:10.1016/j.str.2016.07.008

Perez-Riverol, Y., Csordas, A., Bai, J., Bernal-Llinares, M., Hewapathirana, S., Kundu, D. J., . . . Vizcaino, J. A. (2019). The PRIDE database and related tools and resources in 2019: improving support for quantification data. *Nucleic Acids Res, 47*(D1), D442-D450. doi:10.1093/nar/gky1106

Prudova, A., Gocheva, V., Auf dem Keller, U., Eckhard, U., Olson, O. C., Akkari, L., . . . Overall, C. M. (2016). TAILS N-Terminomics and Proteomics Show Protein Degradation Dominates over Proteolytic Processing by Cathepsins in Pancreatic Tumors. *Cell Rep, 16*(6), 1762-1773. doi:10.1016/j.celrep.2016.06.086

Reiner, O., Coquelle, F. M., Peter, B., Levy, T., Kaplan, A., Sapir, T., . . . Bergmann, S. (2006). The evolving doublecortin (DCX) superfamily. *BMC Genomics, 7*, 188. doi:10.1186/1471-2164-7-188

Repnik, U., Stoka, V., Turk, V., & Turk, B. (2012). Lysosomes and lysosomal cathepsins in cell death. *Biochim Biophys Acta, 1824*(1), 22-33. doi:10.1016/j.bbapap.2011.08.016

Rich, D. P., Schworer, C. M., Colbran, R. J., & Soderling, T. R. (1990). Proteolytic activation of calcium/calmodulin-dependent protein kinase II: Putative function in synaptic plasticity. *Mol Cell Neurosci, 1*(2), 107-116. doi:10.1016/1044-7431(90)90013-t

Rosenberg, O. S., Deindl, S., Comolli, L. R., Hoelz, A., Downing, K. H., Nairn, A. C., & Kuriyan, J. (2006). Oligomerization states of the association domain and the holoenyzme of Ca2+/CaM kinase II. *FEBS J, 273*(4), 682-694. doi:10.1111/j.1742-4658.2005.05088.x

Salter, M. W., & Kalia, L. V. (2004). Src kinases: a hub for NMDA receptor regulation. *Nat Rev Neurosci, 5*(4), 317-328. doi:10.1038/nrn1368

nrn1368 [pii]

Sashindranath, M., Daglas, M., & Medcalf, R. L. (2015). Evaluation of gait impairment in mice subjected to craniotomy and traumatic brain injury. *Behav Brain Res, 286*, 33-38. doi:10.1016/j.bbr.2015.02.038

Sashindranath, M., Samson, A. L., Downes, C. E., Crack, P. J., Lawrence, A. J., Li, Q. X., . . . Medcalf, R. L. (2011). Compartment- and context-specific changes in tissue-type plasminogen activator (tPA) activity following brain injury and pharmacological stimulation. *Lab Invest, 91*(7), 1079-1091. doi:10.1038/labinvest.2011.67

Sattler, R., Xiong, Z., Lu, W. Y., Hafner, M., MacDonald, J. F., & Tymianski, M. (1999). Specific coupling of NMDA receptor activation to nitric oxide neurotoxicity by PSD-95 protein. *Science, 284*(5421), 1845-1848. doi:10.1126/science.284.5421.1845

Savitz, S. I., & Fisher, M. (2007). Future of neuroprotection for acute stroke: in the aftermath of the SAINT trials. *Ann Neurol, 61*(5), 396-402. doi:10.1002/ana.21127

Schaar, B. T., Kinoshita, K., & McConnell, S. K. (2004). Doublecortin microtubule affinity is regulated by a balance of kinase and phosphatase activity at the leading edge of migrating neurons. *Neuron, 41*(2), 203-213. doi:10.1016/s0896-6273(03)00843-2

Shao, G., Wang, Y., Guan, S., Burlingame, A. L., Lu, F., Knox, R., . . . Jiang, X. (2017). Proteomic Analysis of Mouse Cortex Postsynaptic Density following Neonatal Brain Hypoxia-Ischemia. *Dev Neurosci, 39*(1-4), 66-81. doi:10.1159/000456030

Shin, E., Kashiwagi, Y., Kuriu, T., Iwasaki, H., Tanaka, T., Koizumi, H., . . . Okabe, S. (2013). Doublecortin-like kinase enhances dendritic remodelling and negatively regulates synapse maturation. *Nat Commun, 4*, 1440. doi:10.1038/ncomms2443

Shinkai-Ouchi, F., Koyama, S., Ono, Y., Hata, S., Ojima, K., Shindo, M., . . . Sorimachi, H. (2016). Predictions of Cleavability of Calpain Proteolysis by Quantitative Structure-Activity Relationship Analysis Using Newly Determined Cleavage Sites and Catalytic Efficiencies of an Oligopeptide Array. *Mol Cell Proteomics, 15*(4), 1262-1280. doi:10.1074/mcp.M115.053413

Shioda, N., Moriguchi, S., Shirasaki, Y., & Fukunaga, K. (2006). Generation of constitutively active calcineurin by calpain contributes to delayed neuronal death following mouse brain ischemia. *J Neurochem, 98*(1), 310-320. doi:10.1111/j.1471-4159.2006.03874.x

Shu, T., Tseng, H. C., Sapir, T., Stern, P., Zhou, Y., Sanada, K., . . . Tsai, L. H. (2006). Doublecortin-like kinase controls neurogenesis by regulating mitotic spindles and M phase progression. *Neuron, 49*(1), 25-39. doi:10.1016/j.neuron.2005.10.039

Simon, R. P., Swan, J. H., Griffiths, T., & Meldrum, B. S. (1984). Blockade of N-methyl-D-aspartate receptors may protect against ischemic damage in the brain. *Science, 226*(4676), 850-852.

Song, J., Wang, Y., Li, F., Akutsu, T., Rawlings, N. D., Webb, G. I., & Chou, K. C. (2019). iProt-Sub: a comprehensive package for accurately mapping and predicting protease-specific substrates and cleavage sites. *Brief Bioinform, 20*(2), 638-658. doi:10.1093/bib/bby028

Sumi, T., Imasaki, T., Aoki, M., Sakai, N., Nitta, E., Shirouzu, M., & Nitta, R. (2018). Structural Insights into the Altering Function of CRMP2 by Phosphorylation. *Cell Struct Funct, 43*(1), 15-23. doi:10.1247/csf.17025

Sun, H. S., Doucette, T. A., Liu, Y., Fang, Y., Teves, L., Aarts, M., . . . Tymianski, M. (2008). Effectiveness of PSD95 inhibitors in permanent and transient focal ischemia in the rat. *Stroke, 39*(9), 2544-2553. doi:10.1161/STROKEAHA.107.506048

Szklarczyk, D., Gable, A. L., Lyon, D., Junge, A., Wyder, S., Huerta-Cepas, J., . . . Mering, C. V. (2019). STRING v11: protein-protein association networks with increased coverage, supporting functional discovery in genome-wide experimental datasets. *Nucleic Acids Res, 47*(D1), D607-D613. doi:10.1093/nar/gky1131

Taus, T., Kocher, T., Pichler, P., Paschke, C., Schmidt, A., Henrich, C., & Mechtler, K. (2011). Universal and confident phosphorylation site localization using phosphoRS. *J Proteome Res, 10*(12), 5354-5362. doi:10.1021/pr200611n

Tominaga, K., Nakanishi, H., Yasuda, Y., & Yamamoto, K. (1998). Excitotoxin-induced neuronal death is associated with response of a unique intracellular aspartic proteinase, cathepsin E. *J Neurochem, 71*(6), 2574-2584. doi:10.1046/j.1471-4159.1998.71062574.x

Tukey, J. W. (1977). Exploratory data analysis, Addison-Wesley.

Tullis, J. E., Buonarati, O. R., Coultrap, S. J., Bourke, A. M., Tiemeier, E. L., Kennedy, M. J., . . . Bayer, K. U. (2021). GluN2B S1303 phosphorylation by CaMKII or DAPK1: no indication for involvement in ischemia or LTP. *iScience, 24*(10), 103214. doi:10.1016/j.isci.2021.103214

Tyanova, S., & Cox, J. (2018). Perseus: A Bioinformatics Platform for Integrative Analysis of Proteomics Data in Cancer Research. *Methods Mol Biol, 1711*, 133-148. doi:10.1007/978-1-4939-7493-1_7

Tyanova, S., Temu, T., Sinitcyn, P., Carlson, A., Hein, M. Y., Geiger, T., . . . Cox, J. (2016). The Perseus computational platform for comprehensive analysis of (prote)omics data. *Nat Methods, 13*(9), 731-740. doi:10.1038/nmeth.3901

Uchida, Y., Ohshima, T., Sasaki, Y., Suzuki, H., Yanai, S., Yamashita, N., . . . Goshima, Y. (2005). Semaphorin3A signalling is mediated via sequential Cdk5 and GSK3beta phosphorylation of CRMP2: implication of common phosphorylating mechanism underlying axon guidance and Alzheimer's disease. *Genes Cells, 10*(2), 165-179. doi:10.1111/j.1365-2443.2005.00827.x

Wakatsuki, S., Saitoh, F., & Araki, T. (2011). ZNRF1 promotes Wallerian degeneration by degrading AKT to induce GSK3B-dependent CRMP2 phosphorylation. *Nat Cell Biol, 13*(12), 1415-1423. doi:10.1038/ncb2373

Wang, J., Liu, S., Fu, Y., Wang, J. H., & Lu, Y. (2003). Cdk5 activation induces hippocampal CA1 cell death by directly phosphorylating NMDA receptors. *Nat Neurosci, 6*(10), 1039-1047. doi:10.1038/nn1119

Wang, K. K., Nath, R., Posner, A., Raser, K. J., Buroker-Kilgore, M., Hajimohammadreza, I., . . . Yuen, P. (1996). An alpha-mercaptoacrylic acid derivative is a selective nonpeptide cell-permeable calpain inhibitor and is neuroprotective. *Proc Natl Acad Sci U S A, 93*(13), 6687-6692.

Wang, T., Ma, G., Ang, C. S., Korhonen, P. K., Stroehlein, A. J., Young, N. D., . . . Gasser, R. B. (2020). The developmental phosphoproteome of Haemonchus contortus. *J Proteomics, 213*, 103615. doi:10.1016/j.jprot.2019.103615

Wang, W., Zhang, F., Li, L., Tang, F., Siedlak, S. L., Fujioka, H., . . . Wang, X. (2015). MFN2 couples glutamate excitotoxicity and mitochondrial dysfunction in motor neurons. *J Biol Chem, 290*(1), 168-182. doi:10.1074/jbc.M114.617167

Wang, Y., Briz, V., Chishti, A., Bi, X., & Baudry, M. (2013). Distinct roles for mu-calpain and m-calpain in synaptic NMDAR-mediated neuroprotection and extrasynaptic NMDAR-mediated neurodegeneration. *J Neurosci, 33*(48), 18880-18892. doi:10.1523/JNEUROSCI.3293-13.2013

Wilson, S. M., Ki Yeon, S., Yang, X. F., Park, K. D., & Khanna, R. (2014). Differential regulation of collapsin response mediator protein 2 (CRMP2) phosphorylation by GSK3ss and CDK5 following traumatic brain injury. *Front Cell Neurosci, 8*, 135. doi:10.3389/fncel.2014.00135

Wu, H. Y., Tomizawa, K., Oda, Y., Wei, F. Y., Lu, Y. F., Matsushita, M., . . . Matsui, H. (2004). Critical role of calpain-mediated cleavage of calcineurin in excitotoxic neurodegeneration. *J Biol Chem, 279*(6), 4929-4940. doi:10.1074/jbc.M309767200

M309767200 [pii]

Yamashima, T., Kohda, Y., Tsuchiya, K., Ueno, T., Yamashita, J., Yoshioka, T., & Kominami, E. (1998). Inhibition of ischaemic hippocampal neuronal death in primates with cathepsin B inhibitor CA-074: a novel strategy for neuroprotection based on 'calpain-cathepsin hypothesis'. *Eur J Neurosci, 10*(5), 1723-1733.

Yoshimura, T., Kawano, Y., Arimura, N., Kawabata, S., Kikuchi, A., & Kaibuchi, K. (2005). GSK-3beta regulates phosphorylation of CRMP-2 and neuronal polarity. *Cell, 120*(1), 137-149. doi:10.1016/j.cell.2004.11.012

Yuasa-Kawada, J., Suzuki, R., Kano, F., Ohkawara, T., Murata, M., & Noda, M. (2003). Axonal morphogenesis controlled by antagonistic roles of two CRMP subtypes in microtubule organization. *Eur J Neurosci, 17*(11), 2329-2343. doi:10.1046/j.1460-9568.2003.02664.x

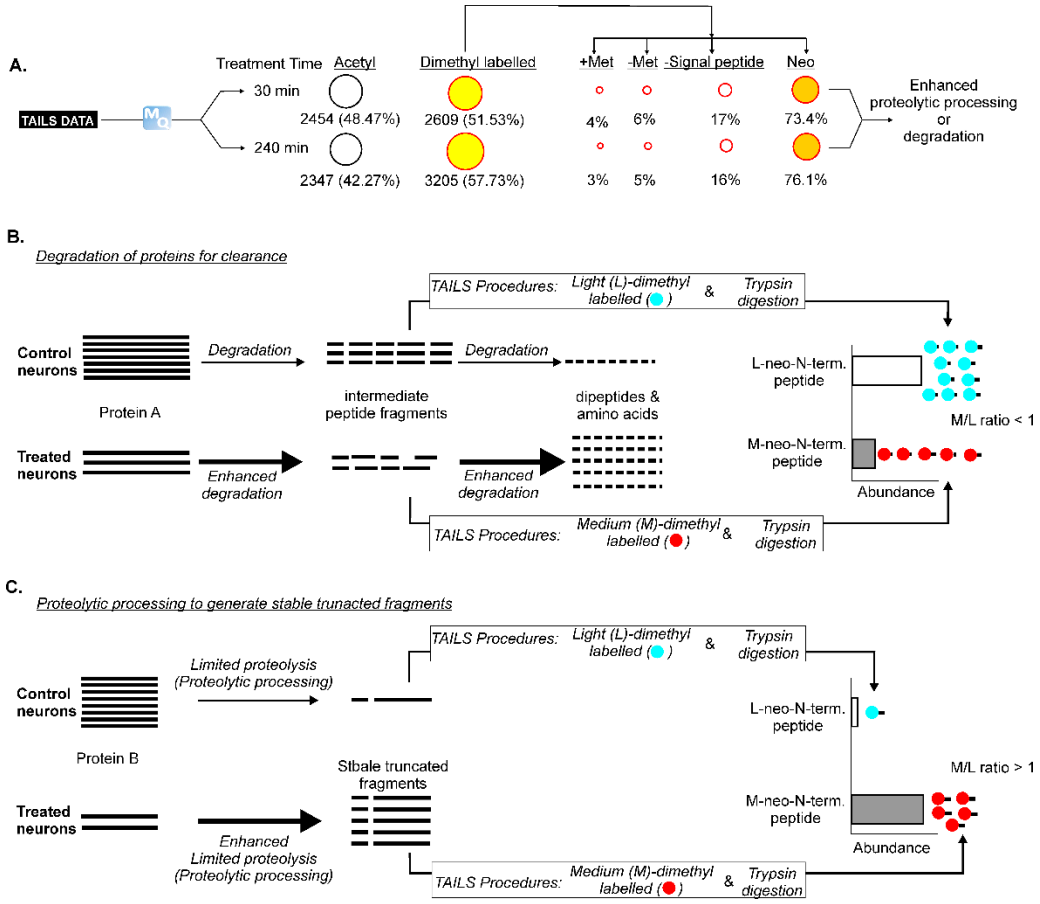

Figure 1 Classification of identified N-terminal peptides derived from neuronal proteins
A. The search engine Andromeda of MaxQuant (MQ) was used to identify and quantify the N-terminal peptides derived from tryptic digests of the neuronal cell lysates in the TAILS method. The identified N-terminal peptides were classified into those with acetylated N-termini and those with free N-termini which were isotopically dimethyl labelled in the TAILS method. The dimethyl-labelled N-terminal peptides were sub-classified into those (i) with intact N-terminal methionine encoded by the start codon (+Met), (ii) with the N-terminal methionine post-translationally deleted *in vivo* (-Met), (iii) with the signal peptide sequence post-translationally deleted by signal peptidases *in vivo* (-Signal peptide) and (iv) with neo-N-termini generated by enhanced proteolysis of neuronal proteins during excitotoxicity (Neo). **B.** Assignment of neo-N-terminal peptides generated by enhanced degradation. The treatment induces a hypothetical protein (Protein A) to undergo enhanced degradation for clearance. It is first proteolyzed to form intermediate peptide fragments, which are then further degraded to form dipeptides and amino acids. In the TAILS procedures, the intermediate peptide fragments are isotopically dimethyl labelled at their neo-N-termini, followed by tryptic digestion to generate the isotopically labelled neo-N-terminal peptides. Since the treatment induces enhanced degradation of the intermediate peptide fragments, the neo-N-terminal peptides derived from Protein A are less abundant in the treated neurons than those in the control neurons (i.e. M/L ratio <1). **C.** Assignment of neo-N-terminal peptides derived from stable protein fragments generated by enhanced proteolytic processing of neuronal proteins. The treatment induces a hypothetical protein (Protein B) to undergo enhanced limited proteolysis (proteolytic processing) to form stable truncated protein fragments. Upon isotopic dimethyl labelling of the neo-N-termini of the truncated protein fragments and tryptic digestion in the TAILS procedures, the resultant labelled neo-N-terminal peptides derived from Protein B are more abundant in the treated neurons than those in the control neurons (i.e. M/L ratio <1).

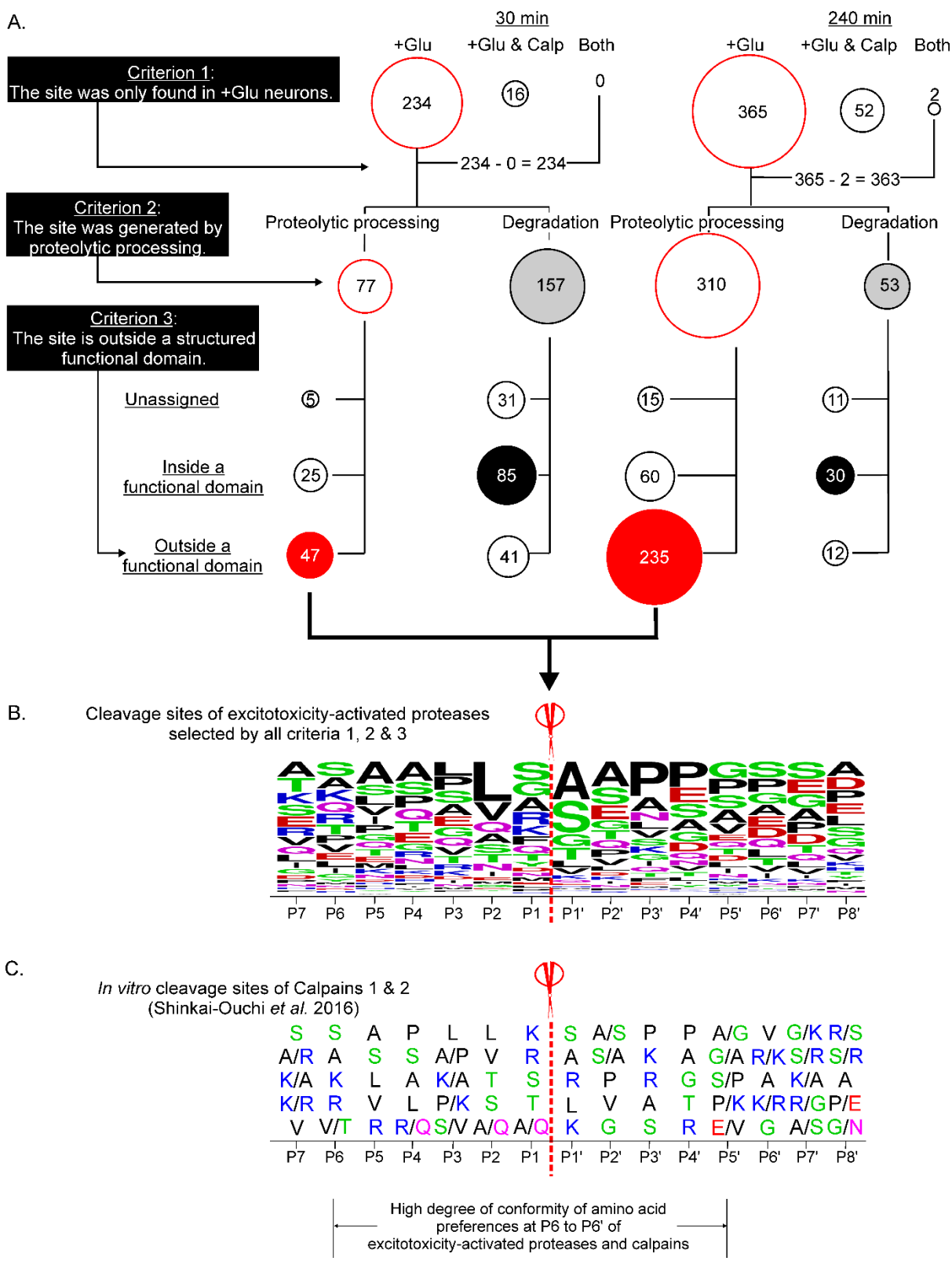
A.
30 min
240 min
+Glu
+Glu & Calp
Both
Criterion 1:
The site was only found in +Glu neurons.
234
16
0
365
52
2
234 - 0 = 234
365 - 2 = 363
Criterion 2:
The site was generated by proteolytic processing.
Proteolytic processing
Degradation
77
157
310
53
Criterion 3:
The site is outside a structured functional domain.
Unassigned
5
31
15
11
Inside a functional domain
25
85
60
30
Outside a functional domain
47
41
235
12
B.
Cleavage sites of excitotoxicity-activated proteases selected by all criteria 1, 2 & 3
P7 P6 P5 P4 P3 P2 P1 P1' P2' P3' P4' P5' P6' P7' P8'
C.
In vitro cleavage sites of Calpains 1 & 2
(Shinkai-Ouchi et al. 2016)
S S A P L L K S A/S P P A/G V G/K R/S
A/R A S S A/P V R A S/A K A G/A R/K S/R S/R
K/A K L A K/A T S R P R G S/P A K/A A
K/R R V L P/K S T L V A T P/K K/R R/G P/E
V V/T R R/Q S/V A/Q A/Q K G S R E/V G A/S G/N
P7 P6 P5 P4 P3 P2 P1 P1' P2' P3' P4' P5' P6' P7' P8'
High degree of conformity of amino acid preferences at P6 to P6' of excitotoxicity-activated proteases and calpains

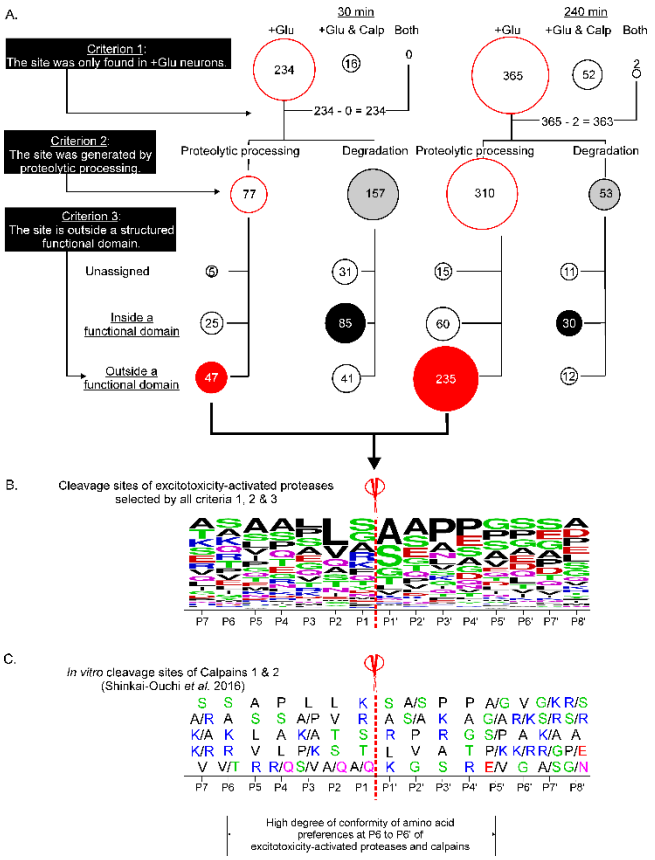

Figure 2 Identification of potential substrates of calpains in excitotoxic neurons

A. Application of the three filtering criteria to predict the neo-N-terminal peptides derived from neuronal proteins cleaved by calpains during excitotoxicity. The criteria were applied to the neo-N-terminal peptides derived from neuronal proteins undergoing enhanced proteolysis induced by glutamate treatment or glutamate/calpeptin co-treatment (Figures S2 and S3). The numbers of significantly changed neo-N-terminal peptides in all treatment groups classified by sequentially applying each of the three filtering criteria are shown and depicted in bubble plots. The bubble size reflects the number of neo-N-terminal peptides. *Bubbles with red perimeter*: the groups of peptides found in glutamate-treated neurons only (Criterion 1) and generated by proteolytic processing (Criterion 2). *Red bubbles*: these peptides fulfilled both Criteria 1 and 2 and the cleavage sites were predicted to reside outside a functional domain (Criterion 3) by the Alpha fold protein structure database to be located outside a functional domain (Criterion 3). Neo-N-terminal peptides fulfilling all three criteria are assigned as those derived from neuronal proteins cleaved by calpains during excitotoxicity. *+Glu only*: peptides identified in glutamate-treated neurons; *+Glu & Calp only*: peptides identified in the glutamate/calpeptin co-treated neurons; *both*: peptides identified in both the glutamate-treated and the glutamate/calpeptin co-treated neurons. **B.** The frequencies of amino acids at positions P7 to P8' proximal to the cleavage sites in the potential calpain substrates (red bubbles). Alignment of the P7-P8' cleavage site sequences of the potential calpain substrates. The amino acid frequencies at each position are represented in WebLogo format (*89*). The sizes of representation of the listed amino acids in each position reflects the frequencies of its appearance in the identified sequences. **(C)** The top five most frequent amino acids at each position in the P7-P8' cleavage site sequences in the synthetic peptides proteolyzed by calpain 1 and calpain 2 *in vitro* (*27*). The amino acids are presented from top to bottom in order of preference with the top-ranked most frequently encountered amino acid residue listed at the top and the fifth ranked frequently encountered residues listed at the bottom. The positions (P6-P5') in the cleavage site sequences where both the excitotoxicity-activated proteases and calpains exhibit high conformity of amino acid preferences are shown at the bottom of panel B. Red: D and E; blue: K, R and H; black: ALVIPM; purple: Q and N; Green: S, T and G.

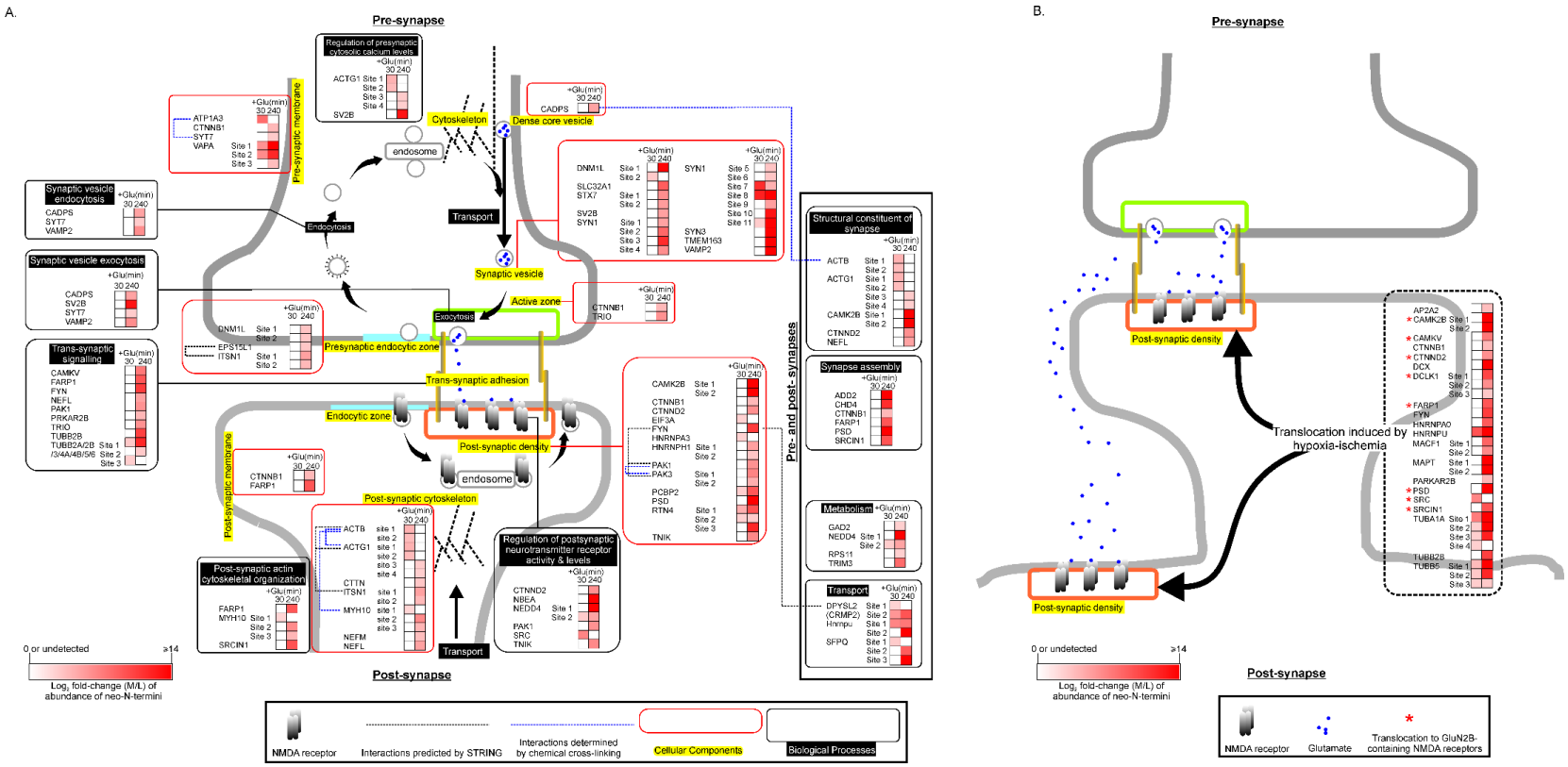
A.
Pre-synapse
Regulation of presynaptic cytosolic calcium levels
+Glu(min)
30 240
ACTG1 Site 1
Site 2
Site 3
Site 4
SV2B
ATP1A3
CTNNB1
SYT7
VAPA
Site 1
Site 2
Site 3
Pre-synaptic membrane
Cytoskeleton
Dense core vesicle
CADPS
endosome
Synaptic vesicle endocytosis
CADPS
SYT7
VAMP2
Endocytosis
Transport
Synaptic vesicle
Synaptic vesicle exocytosis
CADPS
SV2B
SYT7
VAMP2
DNM1L
SLC32A1
STX7
SV2B
SYN1
SYN1
SYN3
TMEM163
VAMP2
Active zone
Exocytosis
CTNNB1
TRIO
DNM1L
EPS15L1
ITSN1
Presynaptic endocytic zone
Trans-synaptic signaling
CAMKV
FARP1
FYN
NEFL
PAK1
PRKAR2B
TRIO
TUBB2B
TUBB2A/2B
/3/4A/4B/5/6
Trans-synaptic adhesion
Endocytic zone
Post-synaptic density
CAMK2B
CTNND2
EIF3A
FYN
HNRNPA3
HNRNPH1
PAK1
PAK3
PCBP2
PSD
RTN4
TNIK
Pre- and post-synapses
Structural constituent of synapse
ACTB
ACTG1
CAMK2B
CTNND2
NEFL
Synapse assembly
ADD2
CHD4
CTNNB1
FARP1
PSD
SRCIN1
Metabolism
GAD2
NEDD4
RPS11
TRIM3
Transport
DPYSL2
(CRMP2)
Hnrnpu
SFPQ
CTNNB1
FARP1
Post-synaptic membrane
endosome
Post-synaptic cytoskeleton
ACTB
ACTG1
CTTN
ITSN1
MYH10
NEFM
NEFL
Post-synaptic actin cytoskeletal organization
FARP1
MYH10
SRCIN1
Transport
Regulation of postsynaptic neurotransmitter receptor activity & levels
CTNND2
NBEA
NEDD4
PAK1
SRC
TNIK
0 or undetected
≥14
Log2 fold-change (M/L) of abundance of neo-N-termini
Post-synapse
NMDA receptor
Interactions predicted by STRING
Interactions determined by chemical cross-linking
Cellular Components
Biological Processes
B.
Pre-synapse
Post-synaptic density
Translocation induced by hypoxia-ischemia
Post-synaptic density
AP2A2
CAMK2B
CAMKV
CTNNB1
CTNND2
DCX
DCLK1
FARP1
FYN
HNRNPAO
HNRNPU
MACF1
MAPT
PARKAR2B
PSD
SRC
SRCIN1
TUBA1A
TUBB2B
TUBB5
0 or undetected
≥14
Log2 fold-change (M/L) of abundance of neo-N-termini
Post-synapse
NMDA receptor
Glutamate
Translocation to GluN2B-containing NMDA receptors

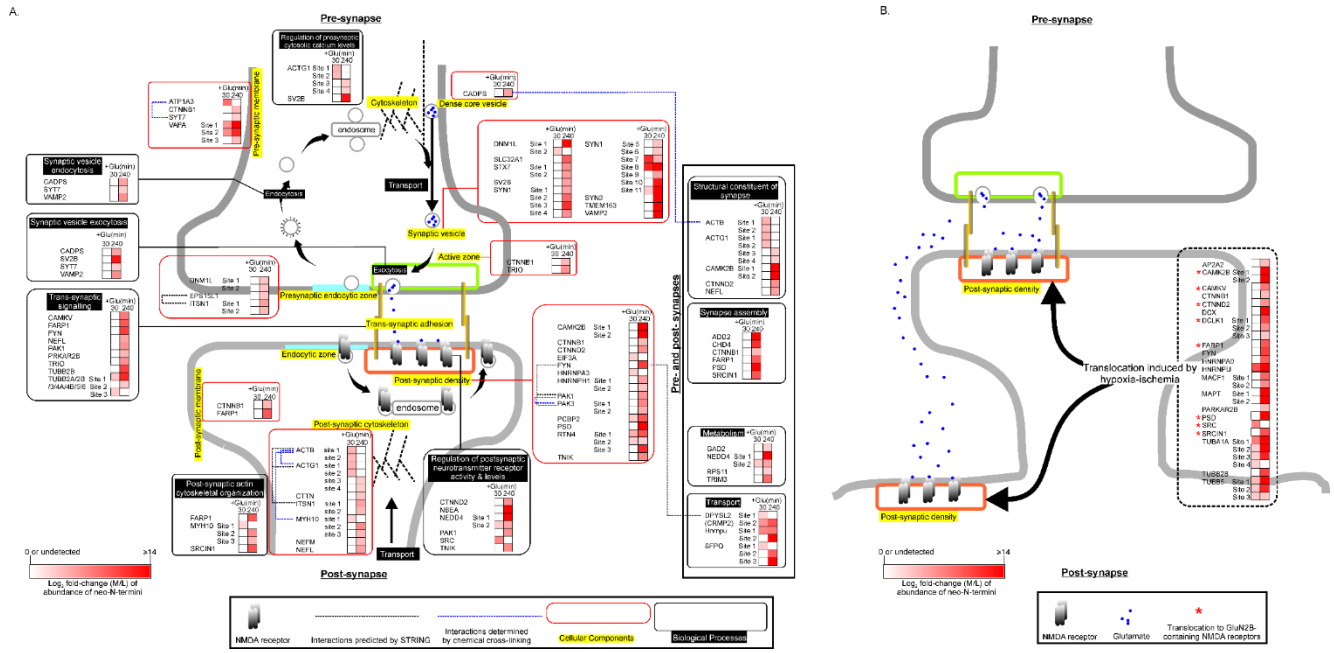

Figure 3 Functions and synaptic locations of proteolytically processed neuronal proteins
A. Neuronal proteins undergoing significantly enhanced proteolytic processing were analyzed by SynGO for their synaptic locations (highlighted in yellow and grouped in red boxes) and biological processes (white fonts in black background and grouped in black boxes). The heatmaps show the abundance ratios of the neo-N-terminal peptides found in glutamate-treated neurons versus those found in control neurons (presented as Log_2-normalized M/L ratio). Neo-N-terminal peptides either undetected or showing no significant changes in abundance at one of the two time points are depicted in white in the heatmaps while those showing a significant increase are in red. Proteins forming complexes identified by cross-linking mass spectrometry by Gonzalez-Lozano, *et al.* (*30*) are linked by blue dotted lines. Proteins forming complexes documented in STRING and with the complex formation confirmed experimentally are linked by black dotted lines. STRING parameters for analysis of the interaction networks are (i) network type: physical subnetwork, (ii) meaning of network edges: evidence, (iii) active interaction sources: experiment and database and (iv) minimum required interaction score: highest confidence (0.900).
B. Synaptic proteins recruited to postsynaptic density in neonatal mouse brain cortex following hypoxia-ischemia (*33, 34*). Red asterisks: synaptic proteins recruited to the GluN2B-containing NMDA receptors (*33*).

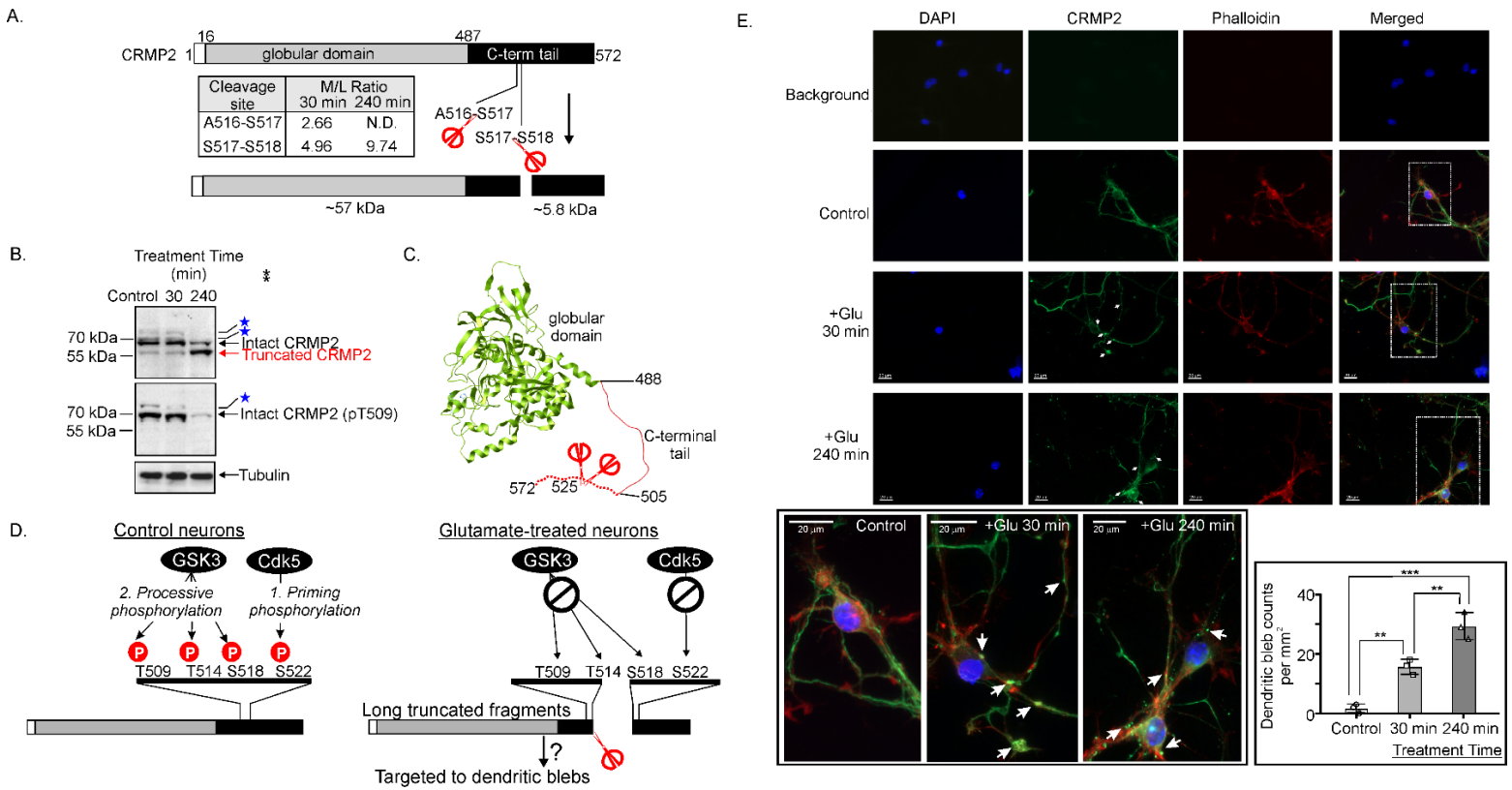
A.
CRMP2
1
16
487
572
globular domain
C-term tail
Cleavage site
M/L Ratio
30 min
240 min
A516-S517
2.66
N.D.
S517-S518
4.96
9.74
A516-S517
S517-S518
~57 kDa
~5.8 kDa
B.
Treatment Time (min)
Control
30
240
70 kDa
55 kDa
Intact CRMP2
Truncated CRMP2
Intact CRMP2 (pT509)
Tubulin
C.
globular domain
488
C-terminal tail
572
525
505
D.
Control neurons
GSK3
Cdk5
2. Processive phosphorylation
1. Priming phosphorylation
T509
T514
S518
S522
Glutamate-treated neurons
Long truncated fragments
?
Targeted to dendritic blebs
E.
DAPI
CRMP2
Phalloidin
Merged
Background
Control
+Glu 30 min
+Glu 240 min
20 µm
Control
+Glu 30 min
+Glu 240 min
Dendritic bleb counts per mm²
40
20
0
***
**
**
Control
30 min
240 min
Treatment Time

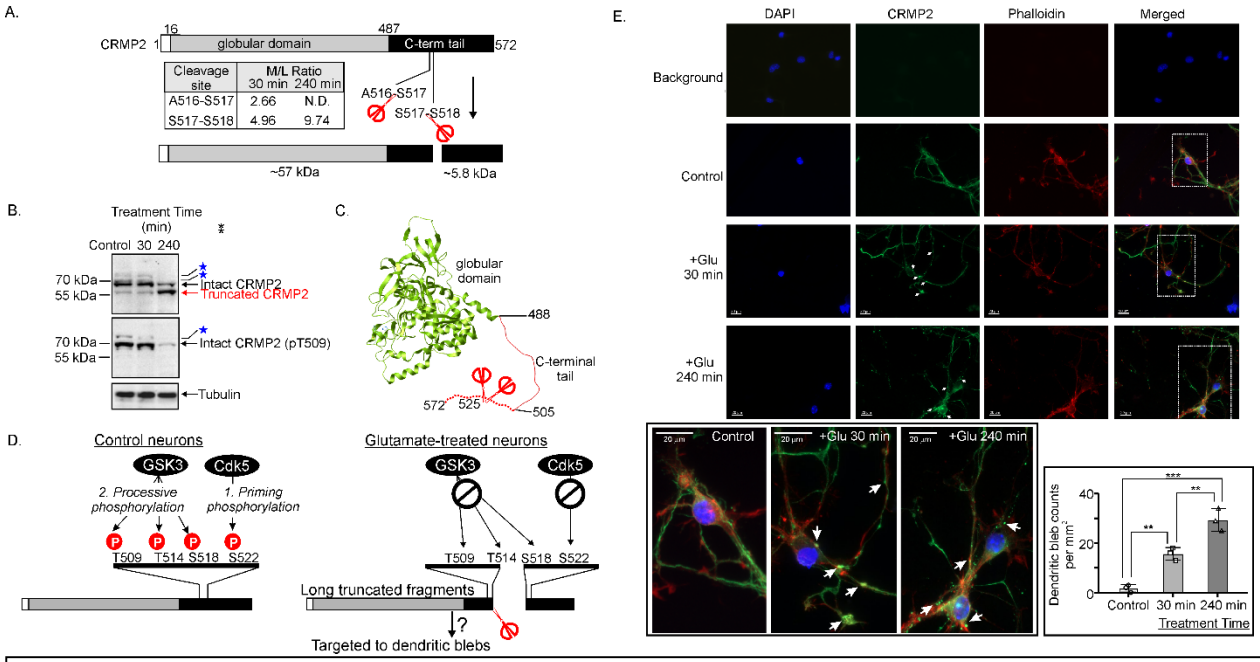

Figure 4 A new mechanism of dysregulation of neuronal CRMP2 (DPYSL2) during excitotoxicity
A. CRMP2 is cleaved at sites in its C-terminal tail. Inset: the abundance (M/L) ratios of the neo-N-terminal peptides at 30 and 240 min after glutamate treatment. *N.D.*: not detected. *Red scissors*: cleavage sites. **B.** Western blots of lysates from control and glutamate-treated neurons probed with anti-CRMP2, anti-pT509 CRMP2 and tubulin antibodies. *Blue stars*: potential hyper-phosphorylated forms of intact CRMP2 detected by the anti-CRMP2 and anti-pT509 CRMP2 antibodies. **C.** Structure of a phosphomimetic mutant of CRMP2 (PDB accession: 5yz5). The dotted line represents the disordered C-terminal tail region. **D.** A model depicting the new mechanism of dysregulation of neuronal CRMP2 during excitotoxicity uncovered by our findings. In control neurons, CRMP2 undergoes hierarchical phosphorylation by Cdk5 and GSK3 at sites in the C-terminal tail. Cdk5 phosphorylates the priming site S522. Upon phosphorylation, pS522 binds GSK3, which catalyzes processive phosphorylation of CRMP2 at three other sites in the order of S518, T514 and T509. In excitotoxic neurons, cleavage of CRMP2 generates a long truncated CRMP2 fragment that lacks the priming site S522, abolishing S522 phosphorylation by Cdk5 and in turn suppressing processive phosphorylation of S518, T514 and T509 by GSK3. The truncation and lack of phosphorylation at T509, T514 and S518 may contribute to the accumulation of the immunoreactive CRMP2 signals at the dendritic blebs shown in *panel E*. **E.** Fluorescence microscopy images showing actin (phalloidin), CRMP2 and nuclei (DAPI) in control and glutamate-treated neurons. *White arrows*: dendritic blebs. *White dotted rectangles*: close-up views of the images shown in *left inset*. *Right Inset*: The number of dendritic blebs per mm^2 in control and the glutamate treated neurons in three biological replicates. Results are presented as mean ± SD; **: $p < 0.01$, ***: $p < 0.001$, one-way ANOVA with Dunnett's multiple comparison test.

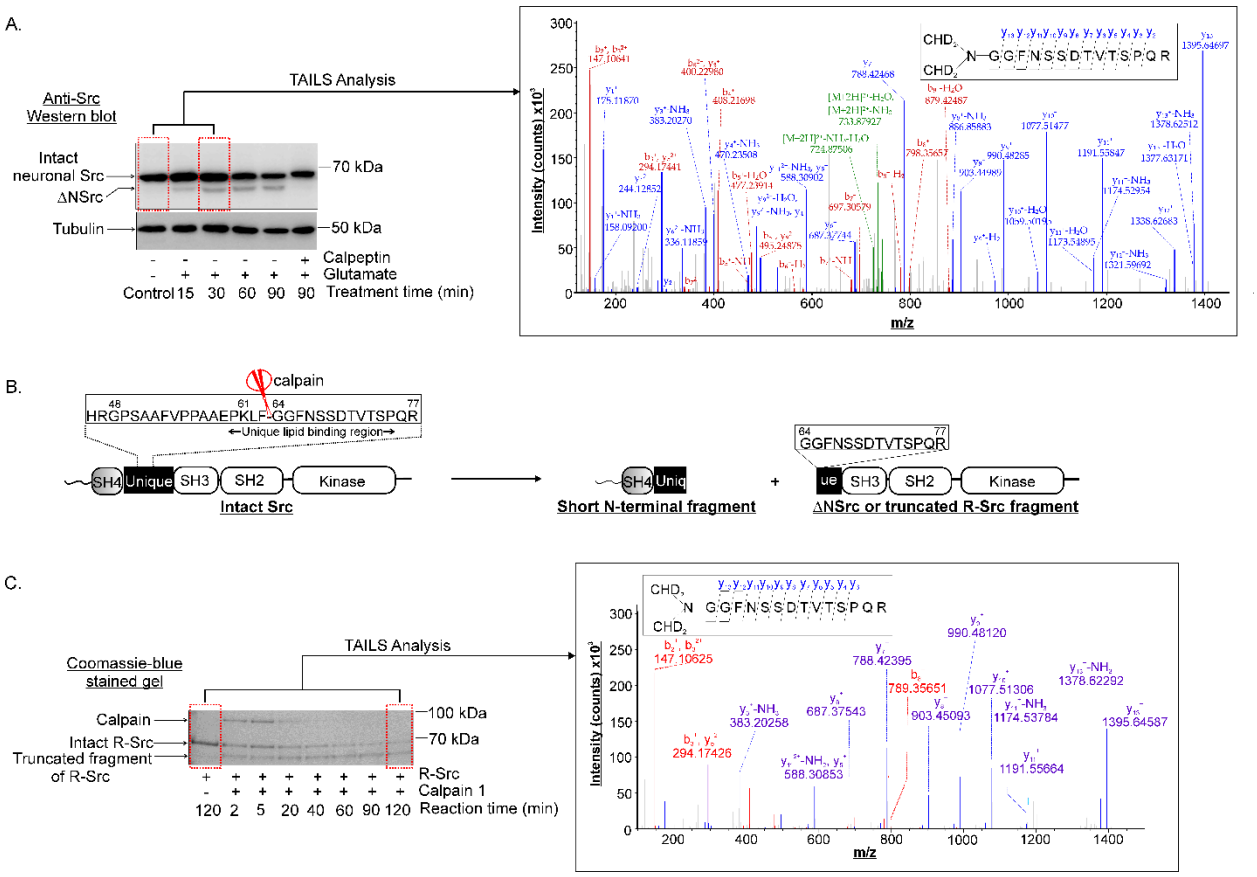

Figure 5 Determination of the calpain cleavage site of Src in glutamate-treated neurons and *in vitro* **(A)** Left panel: Western blot of neuronal Src in control neurons, glutamate-treated neurons and glutamate/calpeptin co-treated neurons. *ΔNSrc*: the long C-terminal fragment generated by calpain cleavage. Right panel: Fragment ion chromatogram identifying a neo-N-terminal peptide encompassing residues 54 to 77 of neuronal Src (*inset*) detectable exclusively in neurons treated with glutamate for 30 min. *Blue*: y ions, *Red*: b ions. **(B)** Schematic diagram depicting the functional domains of intact Src and the calpain cleavage site (*red scissors*) and formation of a short N-terminal fragment and ΔNSrc by calpain cleavage. The cleavage site is mapped to the Unique Lipid Binding Region in the Unique domain. Hence, ΔNSrc lacks the ability to bind plasma membrane. **(C)** Right panel: Coomassie blue-stained SDS-PAGE gel of reaction mixtures containing recombinant neuronal Src (R-Src) after incubation with Calpain 1 for 2 min to 120 min *in vitro*. *Boxes with dotted red lines*: samples analyzed with the TAILS method. Left panel: The fragment ion chromatogram identifying the deuterated dimethyl-labelled Src (64-77) segment of R-Src as the neo-N-terminal peptide (*inset*) detected only in the reaction mixture containing R-Src and calpain 1 at 120 min of incubation. *Blue*: y ions, *Red*: b ions.

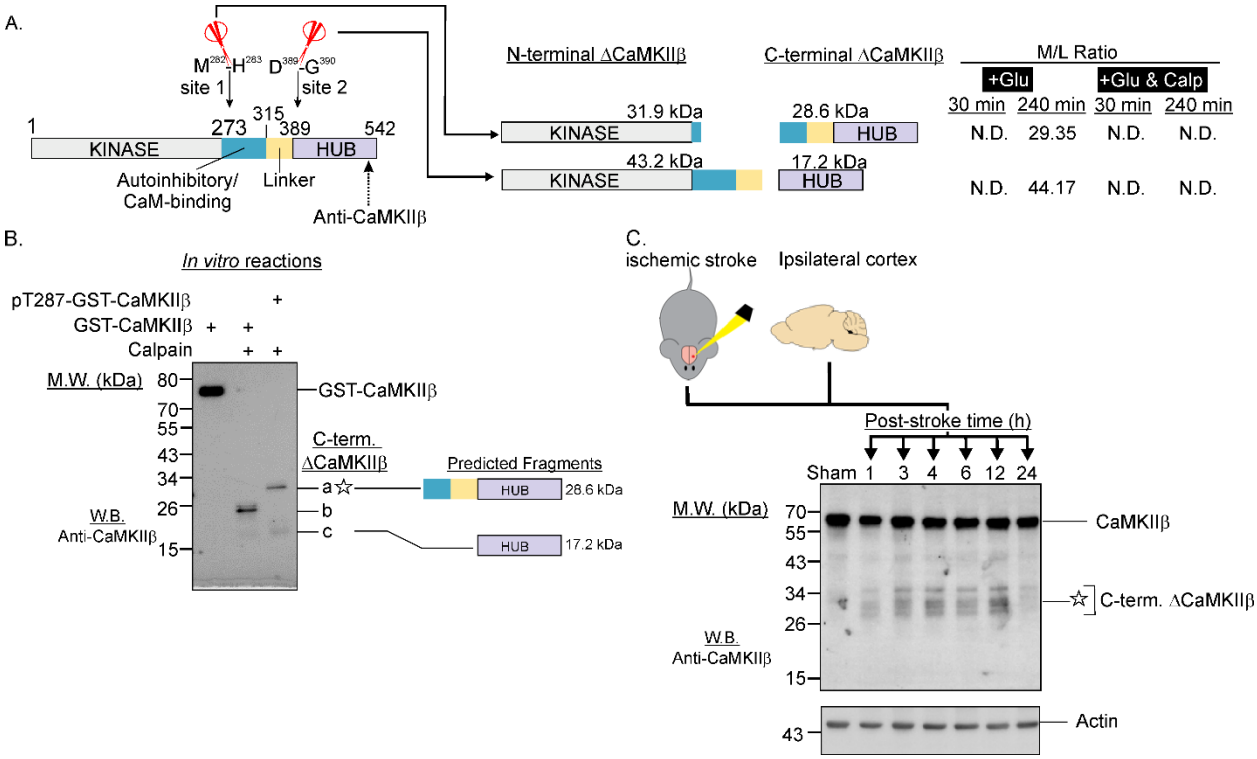

Figure 6 Ischemic stroke induced further proteolytic processing of CaMKIIβ in mouse brain cortex
A. Schematic diagram depicting the cleavage sites in CaMKIIβ undergoing proteolytic processing in glutamate-treated neurons (+Glu) but not in neurons treated with glutamate and calpeptin (+Glu & Calp). *M/L ratio*: ratio of the neo-N-terminal peptide in the treated versus control neurons. *N.D.*: not detected. *Arrow with dotted line*: epitope of anti-CaMKIIβ antibody mapped to the C-terminal hub domain of CaMKIIβ. **B.** Differential cleavage of recombinant GST-CaMKIIβ and pT287 GST-CaMKIIβ by calpain-1. GST-CaMKIIβ with and without prior autophosphorylation at T287 (200 ng of GST-CaMKIIβ plus 100 μM ATP, 10 mM Mg^{2+}, 1.5 Ca^{2+} and 5 μM CaM at 30 °C for 2 min) were incubated with calpain-1 (1 unit) *in vitro* for 45 min). The reaction mixtures were analyzed by Western blotting using the anti-CaMKIIβ antibody. *C-term. ΔCaMKIIβ*: C-terminal fragments of CaMKIIβ generated by calapin cleavage. *Predicted fragments*: Identities of C-term. ΔCaMKIIβ bands a and c predicted from N-terminomic findings shown in *panel A*. **C.** Western blot analysis of brain cortical lysates (20 μg of proteins) of sham-operated mice and mice at designated time points after ischemic stroke using the anti-CaMKIIβ antibody. Among the several C-term. ΔCaMKIIβ bands detected in ischemic stroke mouse brains, the mobility of one of them in SDS-PAGE (marked by a star) was similar to that of band a (marked by a star) in *panel B*.

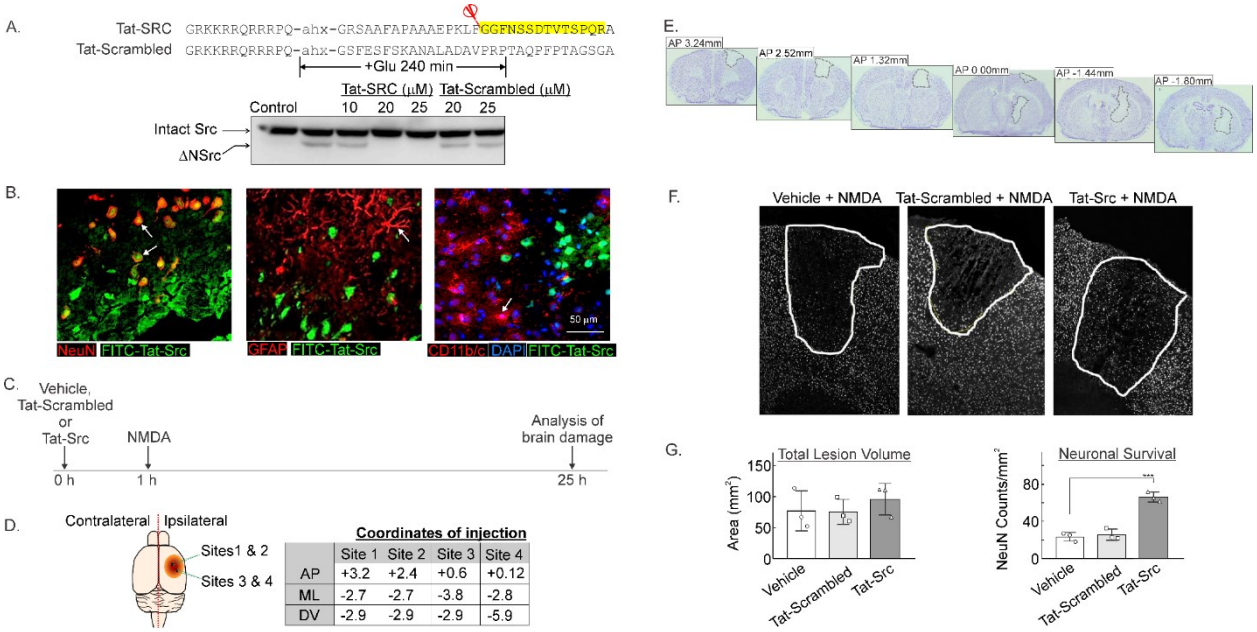

Figure 7 TAT-Src protects against neuronal loss *in vivo* in NMDA-mediated neurotoxicity
(**A**) Tat-SRC but not Tat-Scrambled blocks cleavage of Src in glutamate-treated neurons. *Upper panel*: Sequences of Tat-Src and Tat-scrambled-Src. Segment highlighted in yellow is the neo-N-terminal peptide corresponding to Src(64-77) detected exclusively in glutamate-treated neurons (see Figure 5A). *Red scissor*: site in neuronal Src cleaved by the excitotoxicity-activated proteases in neurons and by calpain 1 *in vitro*. *Lower panel*: Tat-Src or Tat-Scrambled of designated concentrations were added to the culture medium 1 h prior to treatment of cultured neurons with 100 μM glutamate. Cleavage of Src during excitotoxicity was monitored by anti-Src Western blot. *ΔNSrc*: truncated Src fragment. (**B**) Representative photomicrographs of FITC labelled TAT-Src infusion co-labelled against markers of neuronal cells (NeuN+ red); astrocytes (GFAP+; red) and microglia (CD11b/c OX-42+, red) and observed as orange. (**C**) Time line depicting treatment with Vehicle (Milli-Q H_2O, 3 μl), Tat-Src (5 mM in Milli-Q H_2O, 3 μl) or Tat-Scrambled (5 mM in Milli-Q H_2O, 3 μl) at 1 h prior to NMDA-induced excitotoxicity. (**D**) Stereotaxic coordinates of the four injection sites (sites 1 - 4) used to cerebrally inject NMDA to induce excitotoxicity (70 mM in PBS, 1 μl per site). (**E**) Representative thionin-stained coronal images of rat brains infused with NMDA to demonstrate damage to the motor cortex and dorsal striatum. (**F**) NeuN+ cells (transposed white using Image J software) in all three treatment groups. (**G**) *Left panel*: the total lesion volumes in the treatment groups. *Right panel*: the total number NeuN+ cells in each treatment group was point-counted using image J software with the number of surviving neurons within the lesion significantly increased in rats treated with TAT-Src ($p < 0.0001$, n = 3/group, one-way ANOVA) followed by the Bonferroni post-hoc test. Data were analyzed using GraphPad Prism, version 8 and presented as mean ± SD. Statistical significance was defined as $p < 0.05$ for infarct volume and $p < 0.0001$ for NeuN cell count.

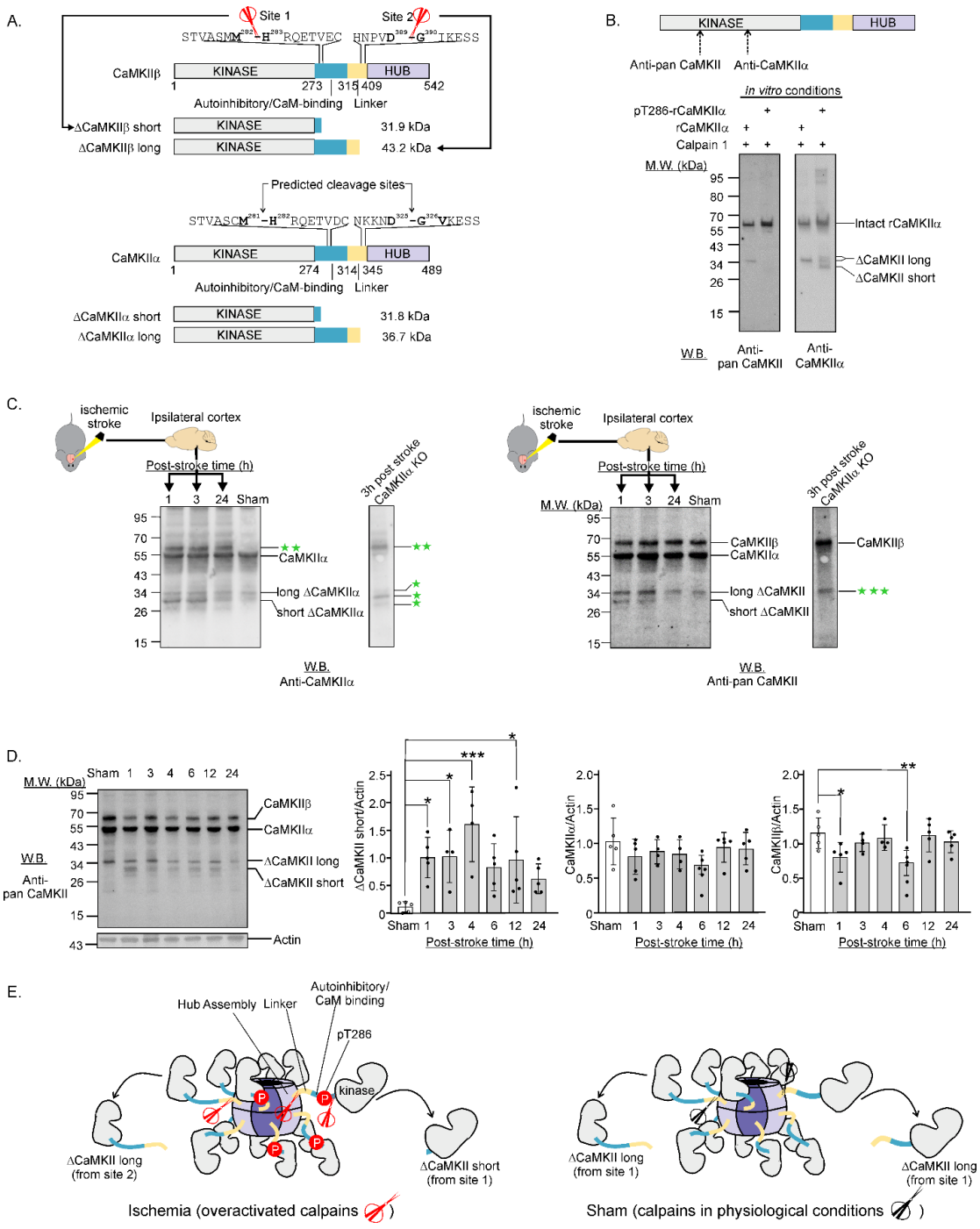
A.
Site 1
Site 2
STVASMM282-H283RQETVEC HNPVD389-G390IKESS
CaMKIIβ
KINASE
HUB
1
273
315
409
542
Autoinhibitory/CaM-binding
Linker
ΔCaMKIIβ short
31.9 kDa
ΔCaMKIIβ long
43.2 kDa
Predicted cleavage sites
STVASCM281-H282RQETVDC NKKND325-G326VKESS
CaMKIIα
1
274
314
345
489
ΔCaMKIIα short
31.8 kDa
ΔCaMKIIα long
36.7 kDa
B.
KINASE
HUB
Anti-pan CaMKII
Anti-CaMKIIα
in vitro conditions
pT286-rCaMKIIα
rCaMKIIα
Calpain 1
M.W. (kDa)
95
80
70
55
43
34
26
15
Intact rCaMKIIα
ΔCaMKII long
ΔCaMKII short
W.B.
Anti-pan CaMKII
Anti-CaMKIIα
C.
ischemic stroke
Ipsilateral cortex
Post-stroke time (h)
1 3 24 Sham
3h post stroke CaMKIIα KO
CaMKIIα
long ΔCaMKIIα
short ΔCaMKIIα
W.B.
Anti-CaMKIIα
M.W. (kDa)
CaMKIIβ
CaMKIIα
long ΔCaMKII
short ΔCaMKII
W.B.
Anti-pan CaMKII
D.
M.W. (kDa)
Sham 1 3 4 6 12 24
CaMKIIβ
CaMKIIα
ΔCaMKII long
ΔCaMKII short
Actin
W.B.
Anti-pan CaMKII
ΔCaMKII short/Actin
CaMKIIα/Actin
CaMKIIβ/Actin
Post-stroke time (h)
E.
Hub Assembly
Linker
Autoinhibitory/ CaM binding
pT286
kinase
ΔCaMKII long (from site 2)
ΔCaMKII short (from site 1)
Ischemia (overactivated calpains)
ΔCaMKII long (from site 1)
ΔCaMKII long (from site 1)
Sham (calpains in physiological conditions)

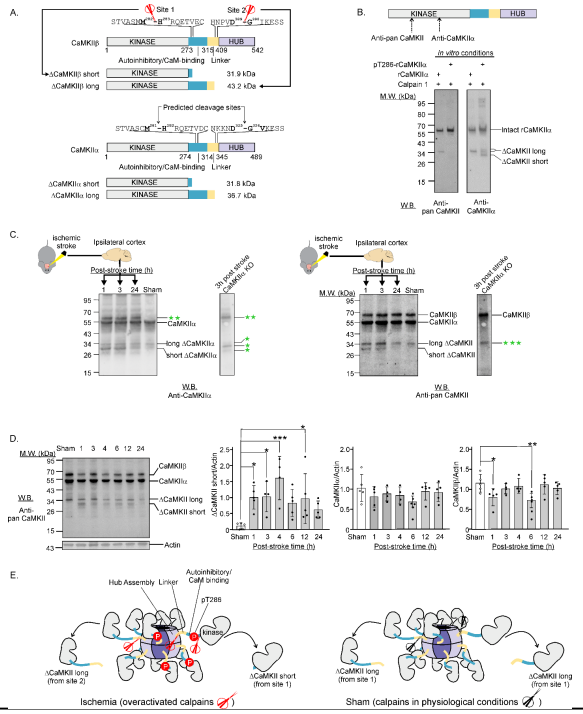

Figure 8: Ischemic stroke induced proteolytic processing of CaMKIIα in mouse brain cortex

A. Calpain cleavage sites of CaMKIIβ in excitotoxic neurons identified by TAILS and the corresponding predicted cleavage sites in CaMKIIα. *ΔCaMKII short and ΔCaMKII long*: N-terminal truncated fragments derived from cleavage at site 1 and site 2, respectively. **B.** Cleavage of unphosphorylated recombinant CaMKIIα (rCaMKIIα) and pT286-rCaMKIIα by calpain-1 *in vitro* generated truncated CaMKIIα (ΔCaMKIIα) fragments with molecular masses similar to those in ischemic stroke mouse brains. The pT286-rCaMKIIα was generated by incubating 200 µg of rCaMKIIα for 2 min at 30 °C in the presence of 10 µM ATP, 10 mM Mg^{2+}, 1.5 mM Ca^{2+} and 5 µM CaM. For the *in vitro* cleavage experiments, rCaMKIIα or pT286-rCaMKIIα was incubated with calpain-1 (1 unit) for 45 min. Reaction mixtures of the *in vitro* experiments were probed with the anti-Pan CaMKII and anti-CaMKIIα antibodies with epitopes mapped to the kinase domain. **C.** Western blots of lysates of brain cortex (20 µg of proteins) collected from wild type sham-operated mice and wild type mice and CaMKIIα KO mice at designated time points after photothrombotic stroke. The blots were probed with anti-CaMKIIα antibody (*left panel*) and anti-pan CaMKII antibody. One green star: Proteins in CaMKIIα KO brain lysates recognized by the anti-CaMKIIα antibody. These proteins were likely the intact and N-terminal proteolytic fragments of other CaMKII isoforms. Two green stars: A protein band cross-reacted with anti-CaMKIIα antibody but not with anti-pan CaMKII antibody. Three green stars: the molecular mass (~35 kDa) of this long N-terminal fragment (ΔCaMKII long) differs from the predicted molecular mass (43.2 kDa) of ΔCaMKII long derived from CaMKIIβ. As this fragment was presented in the CaMKIIα KO brain lysate, it is likely derived from another CaMKII isoform such as CaMKIIδ expressed in brain cells. **D.** Western blot of lysates of brain cortex collected from wild type sham-operated mice and at designated time points after photothrombotic stroke treatment. The blot was probed with anti-pan CaMKII antibody (*left panel*). The abundance ratios of the intact CaMKIIα or CaMKIIβ versus actin and those of the short N terminal fragment of CaMKII (ΔCaMKII short) in brain cortical lysates of sham-operated and ischemic stroke mice (*right panels*). The *p*-values are represented as * for *p*-value < 0.05, ** for *p*-value < 0.01 and *** for *p*-value < 0.001. **E.** A model of differential cleavage of CaMKII oligomer by calpains in sham and ischemic stroke mouse brains. Under physiological conditions, calpains (black scissors) cleave CaMKIIα and CaMKIIβ homo- and hetero-oligomers at site 2 to generate ΔCaMKII long containing the kinase domain, the autoinhibitory/CaM binding motif and the linker motif. In ischemic stroke condition, calpains are over-activated and the CaMKII oligomers undergo autophosphorylation at Thr-286. The over-activated calpains (red scissors) cleave the autophosphorylated CaMKIIα and CaMKIIβ oligomers at sites 1 and 2, respectively to generate ΔCaMKII short and ΔCaMKII long fragments.